Copyright Warning & Restrictions

The copyright law of the United States (Title 17, United States Code) governs the making of photocopies or other reproductions of copyrighted material.

Under certain conditions specified in the law, libraries and archives are authorized to furnish a photocopy or other reproduction. One of these specified conditions is that the photocopy or reproduction is not to be "used for any purpose other than private study, scholarship, or research." If a, user makes a request for, or later uses, a photocopy or reproduction for purposes in excess of "fair use" that user may be liable for copyright infringement,

This institution reserves the right to refuse to accept a copying order if, in its judgment, fulfillment of the order would involve violation of copyright law.

Please Note: The author retains the copyright while the New Jersey Institute of Technology reserves the right to distribute this thesis or dissertation

Printing note: If you do not wish to print this page, then select "Pages from: first page # to: last page #" on the print dialog screen

ABSTRACT

Design of Mask for Striped Filters and Thin-Film Multi-layer Emissivity Modeling for Multi-Wavelength Imaging Pyrometer

by
Jitesh Navinchandra Shah

Multi-Wavelength Imaging Pyrometry (M-WIP) measures thermal radiation of any target (color or gray) in multiple narrow-spectral-regions and can simultaneously determine target temperature and emissivity. One approach for measuring radiation at multiple wavelengths using a 320X244 element Pt-Si SBD infrared camera is to use narrow-band striped filters deposited on a transparent substrate with proper alignment. The major focus of this thesis was the design of a four layer mask for investigating the feasibility of defining three-wavelength striped filters compatible with focal plane array. This mask design allows twelve distinct narrow band striped filter geometries and four test-patterns on a 4-inch silicon wafer.

Prior knowledge of spectral and directional emissivity as a function of thickness of the layer being etched or deposited has extreme importance in improving operating parameters of M-WIP such as selection of spectral range and number of required wavelength. A detailed study of spectral (2.5 μm to 5.0 μm) and directional (0° and 80° from the normal of surface) emissivity variation of thin-film multilayer structure was done, using the developed model, for several important structures commonly used in plasma etching. These multi-layer structures are Poly-Si on thin and thick oxides, silicides on thick oxides and polysides on thin oxides. This analysis can be easily extended to other processing techniques such as sputtering, evaporation, CVD and RTP.

DESIGN OF MASK FOR STRIPED FILTERS
AND
THIN-FILM MULTI-LAYER EMISSIVITY MODELING
FOR
MULTI-WAVELENGTH IMAGING PYROMETER

by

Jitesh Navinchandra Shah

A Thesis
Submitted to the Faculty of
New Jersey Institute of Technology
in Partial Fulfillment of the Requirements for the Degree of
Master of Science in Electrical Engineering

Department of Electrical and Computer Engineering

October 1993

APPROVAL PAGE

Design of Mask for Striped Filters

and

Thin-Film Multi-layer Emissivity Modeling
for
Multi-Wavelength Imaging Pyrometer

Jitesh Navinchandra Shah

Dr. Walter F. Kosonocky, Thesis Advisor — date
Distinguished Professor of Electrical Engineering and Holder of
Foundation Chair in Optoelectronics and Solid-State Circuits, NJIT

Dr. Durgamadhab Misra, Thesis Advisor — date
Associate Professor of Electrical Engineering, NJIT

Dr. Nuggehalli Ravindra, Committee Member — date
Associate Professor of Physics, NJIT

BIOGRAPHICAL SKETCH

Author: Jitesh Navinchandra Shah

Degree: Master of Science in Electrical Engineering

Date: October 1993

Undergraduate and Graduate Education:

- Master of Science in Electrical Engineering,
  New Jersey Institute of Technology, Newark, New Jersey, 1993
- Bachelor of Science in Electrical Engineering,
  Maharaja Sayajirao University, Baroda, INDIA, 1990

Major: Electrical Engineering

Publications :

J. Shah and D. Misra, "Microprocessor based Automation of Reactive Ion Etching (RIE) Process," Submitted to the *IEEE Transaction on Semiconductor Manufacturing*.

V. Patel, J. Shah, W.F. Kosonocky, D. Misra and B. Singh, "Plasma Etching Uniformity and End-point Determination Using Thermal Imaging," To be submitted for publication in the *Journal of Vacuum Science and Technology*.

This thesis is dedicated to

my parents

for all the love and encouragement

Acknowledgment

The author would like to express his sincere gratitude to his thesis advisor, Dr. Walter F. Kosonocky, NJIT Foundation Chair for Optoelectronics and Solid State Circuits., for technical suggestions, important discussions and financial support during this research work. The author is also indebted to his advisor, Dr. Durga Misra, Associate Professor, Electrical and Computer Engineering Department, for his technical assistance, suggestions and initial financial support.

Special thanks are due to Dr. N.M. Ravindra for serving as member of the committee.

The author would like to express his deepest gratitude to Dr. Vipul Patel, NJIT, who spent countless hours on different parts of this thesis work. He gave me continuous courage, important information and moral support without which I could never have finished this work in time.

The author is also grateful to N. McCaffrey and M. Kaplinsky for participating various discussions, troubleshooting the camera electronic circuits and providing important technical information about M-WIP. The author is also grateful to Dr. B. Singh, Dr. L.White and Ms. G. Marray at David Sarnoff Research Center, Princeton, NJ. for providing important technical suggestions during mask design for striped filters.

The author also wishes to express his appreciation to his uncle Dipak and aunt Dipti for providing moral support. Author would like to extend his appreciation to his roommates Sanjay, Shreyansh and Tamaya for their kind help. Author can not forget the timely help and suggestions from his friends and colleagues at the Electronics Imaging Center, including: Dr. D. Shah, M. Berry, Sudesh, Bing, Pan, Yang and Chao Ye.

Table of Contents

Chapter **Page**

List of Tables

List of Figures

Figure **Page**

CHAPTER 1

INTRODUCTION

The research and development work presented in this thesis was performed at the Electronic Imaging Center, NJIT under the guidance of Dr. Walter F. Kosonocky, NJIT Foundation Chair for Optoelectronics and Solid State Circuits, and Dr. Durga Misra, Associate Professor, ECE Department, NJIT. This work was supported by DARPA contract number F33615-92-C-5817 "Multi-Wavelength Imaging Pyrometry (M-WIP) for Semiconductor Process Monitoring and Control".

In most material manufacturing and processing applications, process rates depend exponentially on the temperature so that very precise (~1°C) temperature measurement is necessary for adequate control. Also, with the increasing importance of transient heating process, such as rapid thermal processing (RTP), near real-time measurement of temperature and thermal gradient is required. The most widely used remote temperature measurement technique is known as pyrometry, which is based on the analysis of the radiation emitted from the surface. Multi-Wavelength Imaging Pyrometer (M-WIP) based on a 320x244 Pt-Si Schottky-barrier detector (SBD) infrared Focal Plane Array (FPA) is being developed at NJIT for above applications. One of the approaches for measuring radiation at multiple wavelengths using the Pt-Si SBD infrared camera is to use narrow-band striped filters deposited on a transparent substrate with proper alignment to the imager. The major objective of this thesis work was to design a four layer mask for investigating the feasibility for defining focal plane array compatible three-wavelength striped filters. This mask design allows definition of twelve distinct narrow band striped filter geometries and various test-patterns on a 4-inch silicon wafer.

In many semiconductor processing applications, thin films are being etched or deposited on a substrate material. Prior knowledge of spectral and directional emissivity as a function of thickness of the layer being etched or deposited has extreme importance in

improving operating parameters of M-WIP such as selection of spectral range and number of required wavelength. An emissivity model for multi-layer thin film structure was developed and applied to several multilayer structures commonly used in plasma etching applications. This analysis can be easily extended to other processing techniques such as sputtering, evaporation, CVD and RTP.

Chapter 2 serves as an introduction to various pyrometric techniques with focus on multi-wavelength pyrometry. The 320x244 Pt-Si SBD infrared imager and camera system used for the M-WIP and various approaches to allow detection of radiation in multiple spectral-bands are also described in this chapter.

A detailed design of photolithographic masks for fabrication of multiwavelength narrow-band striped filters is presented in Chapter 3.

Chapter 4 focus on emissivity modeling of various thin-film multi-layer structures commonly used in plasma etching application. Importance of this modeling work to M-WIP application is also described in detailed in this chapter.

Finally, Chapter 5 contains concluding remarks and suggestions for future work.

CHAPTER 2

MULTI-WAVELENGTH IMAGING PYROMETRY(M-WIP) SYSTEM

2.1 Introduction

Accurate measurement and control of temperature is of great importance in most material manufacturing and processing applications. The most widely used remote temperature measurement technique is known as pyrometry, which is based on the analysis of the radiation emitted from the surface. In pyrometry, radiation emitted from a surface is collected on a detector (sensitive in the spectral range of interest) through suitable optics and then the detected signal is related to the temperature of the emitting body by using proper radiometric procedures. The major difficulty in the pyrometric measurement of temperature is the unknown emissivity of the radiant target. Several methods have been used to overcome the problem of unknown emissivity. These methods can be divided into three broad areas. They are: (1) Single-wavelength pyrometry, (2) Two-wavelength (Ratio) pyrometry and (3) Multi-wavelength pyrometry.

Single wavelength pyrometry requires prior knowledge of emissivity in a narrow-spectral region of interest. Two-wavelength pyrometry overcomes the problem of unknown emissivity for gray bodies (gray in the spectral range of interest) by taking a ratio of the detected signal measured in two spectral regions. The temperature measurement accuracy of this technique, however, deteriorates for color bodies with unknown emissivity. In contrast, Multi-Wavelength Pyrometry (MWP) measures radiation in multiple narrow-band spectral regions and can determine temperature without any prior knowledge of emissivity. To date, this technique is used only in conjunction with a single point temperature measurement [1]. Measurement of temperature profiles is of great importance and hence a Multi-Wavelength Imaging Pyrometer (M-WIP) is being developed at NJIT under

supervision of Prof. Kosonocky as an advanced system for real-time *in situ* monitoring and control of semiconductor processes in a manufacturing environment.

In this chapter, fundamental radiometric relations are briefly described first, followed by discussion on advantages and limitations of various pyrometric techniques. Finally, the infrared camera system being used for M-WIP and various approaches for multiple wavelength detection are discussed.

2.2 Blackbody Radiation

Any body at temperature above the absolute zero temperature emits spectral radiation. This radiation characteristic is subject to known laws and is normally represented as a function of blackbody radiation. A blackbody radiator is an idealized source of radiant energy which also absorbs all radiation incident upon it. The blackbody is a perfect diffused radiator with a well-defined radiation spectrum. Since it is possible to build a close approximation of radiation properties of any surface to a blackbody, this concept is a very useful for the calibration and testing of radiometric instruments. The parameter which relates the radiation characteristics of any real body to that of a blackbody is known as emissivity. Emissivity is defined as the ratio of the radiation emitted by the surface to the radiation emitted by a blackbody at the same temperature and for the same spectral and directional conditions. For a blackbody, emissivity is unity under all spectral and directional conditions. Basic concepts of emissivity are described in detail in Chapter 4.

Planck's law relates the spectral radiant emittance (radiance) of a perfect blackbody to its temperature and the wavelength of the emitted radiation. The mathematical expression that describes the Planck's radiation law is given as:

$$L(\lambda,T)=\frac{2hc^2}{\lambda^5}\frac{1}{e^{hc/\lambda kT}-1} \qquad [W\,cm^{-2}\,sr^{-1}\mu m^{-1}] \qquad (2\text{-}1)$$

where h- is Planck's constant, 6.6262 X 10^{-34} Js;

λ- is the wavelength in micrometers;

c- is the velocity of light, 2.997 X 10^{8} m/s;

k- is Boltzmann's constant, 1.3806 X 10^{-23} J/K; and

T- is the absolute temperature in Kelvin (K).

Figure 1 illustrates the spectral distribution of blackbody radiation as a function of wavelength for a selected temperature range [2]. The Planck radiation formula (Eq. 2-1) shows that the spectrum of the radiation shifts toward shorter wavelengths or longer wave numbers as the temperature of the radiator is increased.

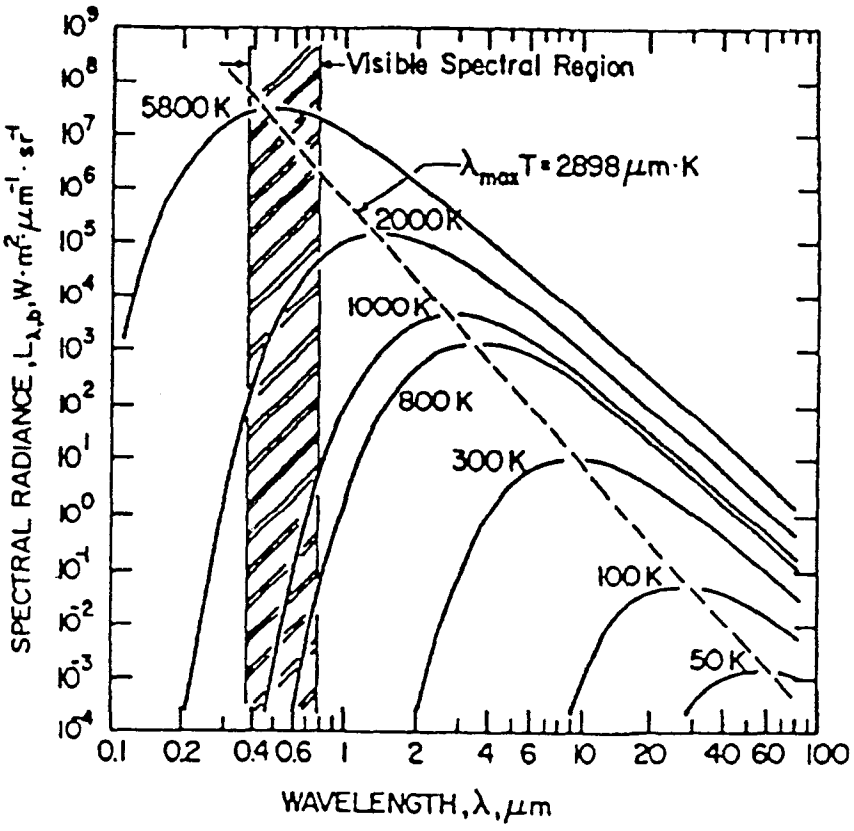

Figure 1 Spectral Radiance of a Blackbody[2].

The total radiation at all wavelengths can be obtained by integrating Eq. 2-1 over the complete spectrum of wavelength. The resulting equation is known as the Stefan-Boltzmann law and is given by:

$$M = \sigma T^4 \quad [W/m^2] \tag{2-2}$$

where σ–is Stefan-Boltzmann constant (5.6697×10^{-8} [$W\ m^{-2}\ K^{-4}$]).

Eq. 2-2 indicates that the total power radiated from a blackbody varies as the fourth power of the absolute temperature. At room temperature (approximately 300K), a perfect blackbody of area equal to 1.0 m^2 emits a total power of 460 W.

For a given temperature, the wavelength at which the spectral radiance ($L\lambda$) is a maximum can be determined by differentiating Eq. 2-1 and the resultant formula is known as the Wien displacement law given as:

$$\lambda_{max} = 2897.8/T \quad [\mu m] \tag{2-3}$$

Eq. 2-3 indicates that the wavelength at which the spectral radiance is a maximum decreases with increasing temperature.

2.3 Pyrometry

Pyrometry techniques are widely used for remote measurement of temperature. They are based on the analysis of the radiation emitted from the surface by using proper radiometric relations described in the previous section. Various pyrometric methods can be divided into three broad areas:

(1) Single-wavelength pyrometry;

(2) Two-wavelength (Ratio) pyrometry; and

(3) Multi-wavelength pyrometry.

2.3.1 Single-Wavelength Pyrometry

It is possible to accurately determine blackbody temperature by measuring the emitted radiation in a spectral band. However, for a color body, temperature can be determined using this method only if emissivity $\varepsilon=\varepsilon(\lambda,T)$ is known. A single narrow or broad spectral-band can be used for detection of radiation from a surface with known emissive characteristics in that spectral band. The monochromatic or single wavelength pyrometry is attractive because it does not require the knowledge of total spectral emissivity. Instead, the emissivity within the detection band or even just at its center wavelength can be used. The broad-band radiometric temperature measurements have the advantage of achieving high signal-to-noise ratio even for relatively low temperatures of radiant target.

2.3.2 Two-Wavelength Ratio Pyrometry

The main source of uncertainty in radiometric temperature measurement is the unknown emissivity (ε). The problem is especially difficult because emissivity is related with the wavelength and temperature in a complex manner. One way to circumvent the problem of unknown emissivity is by measuring radiation at two different wavelengths. The two wavelength pyrometry (generally known as ratio pyrometry) infers the temperature from the ratio of measurements in two different spectral bands (see Figure 2). Although measurement of two signals adds more uncertainty due to the noise present in both measurements, this method can successfully circumvent the problem of unknown emissivity for graybody radiators.

It should be noted that in the case of a graybody radiator with $\varepsilon(\lambda_1) = \varepsilon(\lambda_2)$, the method of ratio radiometry can be used to determine the temperature of a gray body radiator with unknown emissivity. Furthermore, the target need not to be totally gray; it is sufficient for the target to have just two spectral regions where the spectral emissivities are equal or the ratio of emissivity in these spectral regions is known.

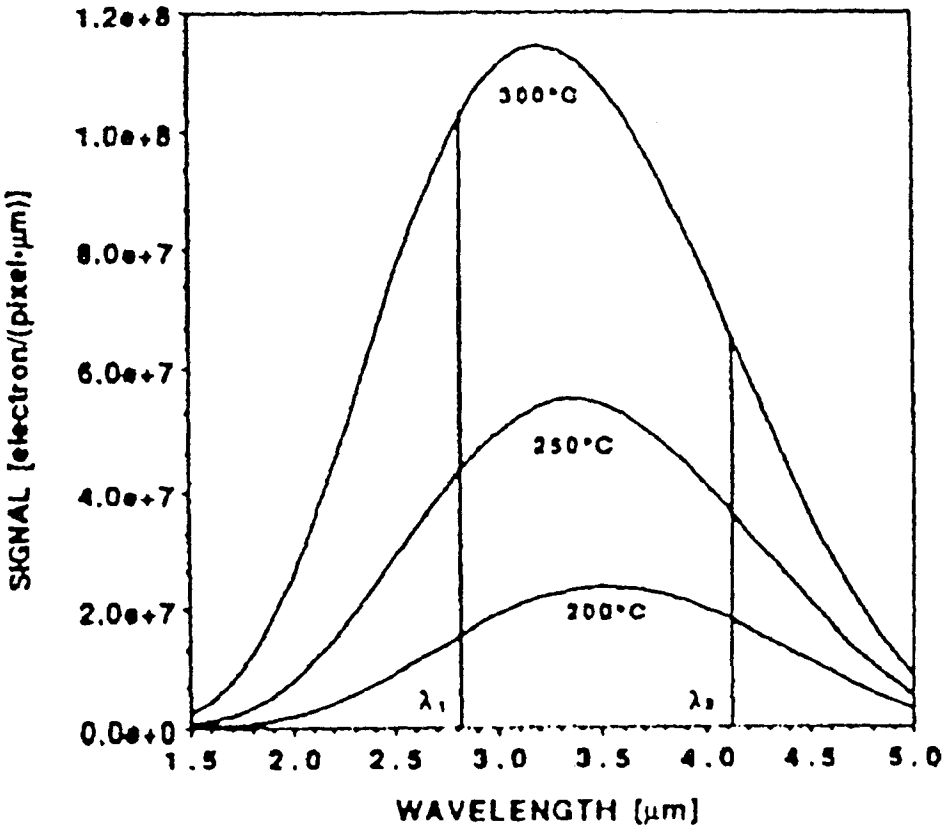

Figure 2 Two wavelength (Ratio) Pyrometry[5].

2.3.3 Multi-Wavelength Pyrometry

As inferred by its name, multi-wavelength pyrometry (MWP) utilizes measurements of the radiation in multiple monochromatic spectral-bands. This technique circumvents the problem of unknown emissivity by assuming a functional dependence of the target spectral emissivity on wavelength. The spectral emissivity in most cases can be adequately represented by a polynomial function of wavelength [3]

$$\varepsilon(\lambda) = a_1 + a_2 \cdot \lambda + a_3 \cdot \lambda^2 + \ldots \qquad (2\text{-}4)$$

where a_1, a_2, a_3,.. are the parameters of the emissivity model.

The detected signal, S, of the detector viewing the target through a narrow-band filter with unknown emissivity (given by Eq. 2-4) can be expressed in a parametric model as

$$S(\lambda, a_1, \ldots, a_{n-1}, T) = K(\lambda) \cdot \varepsilon(\lambda, a_1, \ldots, a_{n-1}) \cdot R(\lambda) \cdot L_{\lambda,b}(\lambda, T) \quad (2\text{-}5)$$

where T(temperature)=a_n- is also an unknown parameter;

K- is filter shape factor; and

R- is the spectral responsivity of the detector.

The central idea of radiometric temperature measurement by MWP is to determine the temperature and the emissivity of the radiant target from the fit of the signal model given by Eq. (2-5) to the set of experimental measurements of the signal, $S_1,\ldots,S_N$ measured at N distinct wavelengths. Interpolation or least-square based techniques can be used for fitting the signal model to the measured signal. However, least square based technique is more preferred due to its higher accuracy[3].

Based on the method of maximum likelihood, it can be shown that the best possible least-squares fit of the given model to the experimental values is achieved when the parameters of the model correspond to the minimum of the following function [4]

$$\min_{a_1,\ldots,a_{n-1},T} \sum_{i=1}^{N} \left\{ \frac{1}{\sigma_i^2} \left[S_i - \tilde{S}(T, \varepsilon, \lambda_i) \right]^2 \right\} \rightarrow a_1, \ldots, a_{n-1}, T \quad (2\text{-}6)$$

Where

S_i - is detected signal at λ_i (electrons / pixel);

S - is theoretical signal at λ_i (electrons /pixel);

T- is temperature of the target (K);

$\varepsilon_i = \varepsilon(\lambda_i) = a_1 + a_2\lambda_i + a_3\lambda_i^2 + \ldots\ldots$ - is the emissivity model; and

$\sigma_i = \Delta S_i = \sqrt{S_i}$ – shot noise.

It should also be noted that in order to obtain meaningful results using least-square fitting, the minimum number of wavelengths, N, should be n+1, where n is the number of unknown parameters of the model. Any additional wavelengths or measurements will improve the accuracy of the technique.

Figure 3 illustrates the concept of MWP indicating least square fit to the simulated detected signals at five different wavelengths. This simulation was performed by M. Kaplinsky for an infrared camera system with a PtSi Schottky-barrier detector array [5]. Simulated target was assumed at 1073K and then detector signal was calculated at five different wavelength ($\lambda 1$ to $\lambda 5$). Linear least square technique was used to curve fit the data and $a_n = T$ was verified.

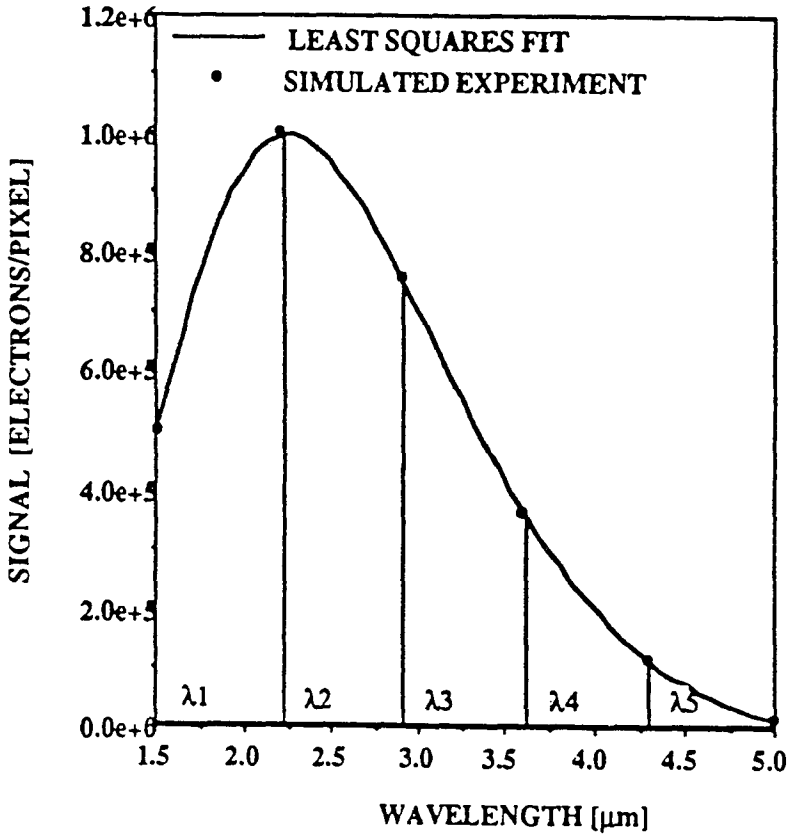

Figure 3 Least-squares fit to the simulated signal detected by a 320x244 IR CCD imager. The fit is based on 8 measurement per filter. The temperature of the simulated target is 1073 K [5].

2.4 Multi-Wavelength Imaging Pyrometer

Multi-Wavelength Imaging Pyrometry refers to measurement of temperature of a scene instead of a single point measurement by using multiple wavelength pyrometry technique. The basic concept of M-WIP is illustrated in Figure 4.

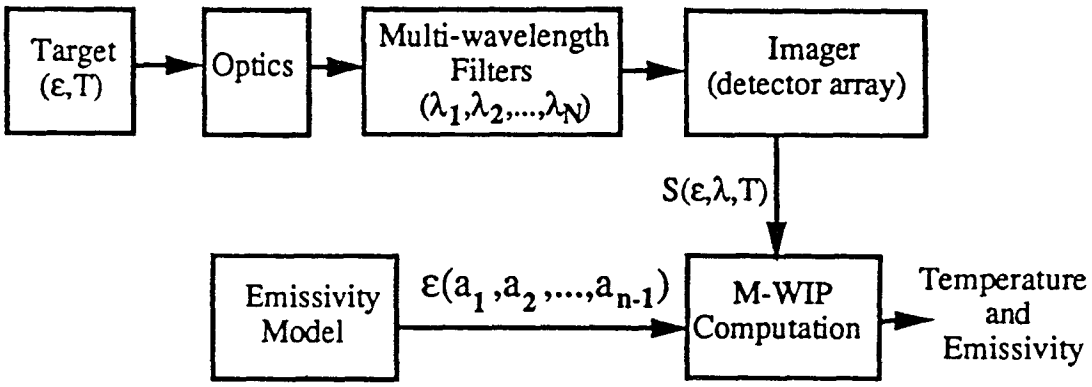

Figure 4 Block diagram representation of the M-WIP system.

The radiation emitted from a surface is detected by a focal plane array imager using proper optics. Using various filter configuration approaches, the radiation can be detected in multiple narrow-spectral-bands by the imager. These multi-wavelength filter approaches and the operation of the 320X244-element PtSi Schottky barrier detector array based infrared camera system are described later in this section. Using multi-wavelength pyrometry technique, the output of the imager can be converted to map the temperature and emissivity of the entire image. It should be noted here that some prior knowledge of spectral emissivity is helpful for selection of emissivity model, spectral range and number of required wavelengths for the M-WIP system. For the application of M-WIP in plasma etching, detailed modeling of emissivity for several multilayer structures was done for the above reason and is presented in Chapter 4.

2.4.1 Choices of Multi-Wavelength Filter Configurations

The multi-wavelength imaging pyrometry technique requires measurements of radiation at multiple monochromatic (sufficiently narrow) spectral-bands. This can be achieved either by temporally or spatially changing the wavelength of detection. There are three practical approaches of filter optics that could be used for the construction of M-WIP system. They are as follows:

(1) A rotating filter wheel that is synchronized with the sequential frame readout of the imaging sensor (FPA);

(2) A beam-splitter and filter assembly that separates the IR image in separate wavelength, each incident on a different IR imager; and

(3) A narrow-band striped filter to form a multi-wavelength IR pyrometer.

The rotating filter wheel (see fig. 5a) represents the most flexible approach that is relatively easy to implement with six or more separate filters. This approach represents temporal change in wavelength of detection and the full resolution of the focal plane array can be utilized. This system can be operated with a stepping motor and will allow a change from filter to filter in about 0.1 s. The requirement of time sequential image sampling tends to limit the application of the rotating filter to the measurements for a relatively slow changing process.

The beam-splitter multi-imager approach (see Fig. 5b) provides the capability for simultaneous multi-wavelength measurements. This approach also can utilize the full resolution of the FPA. However, this approach is expected to be the most expensive and for practical considerations is limited to two or three imagers with separate filters.

The striped filter approach (see Fig. 5c) represents spatial detection of different wavelengths on the focal plane array. In this approach, a set of detectors will be detecting radiation in different spectral bands simultaneously. This approach is capable of achieving high temperature measurement accuracy if the emissivity of the area on scene corresponding to each set of detectors (for example, each set of detectors for M-WIP using

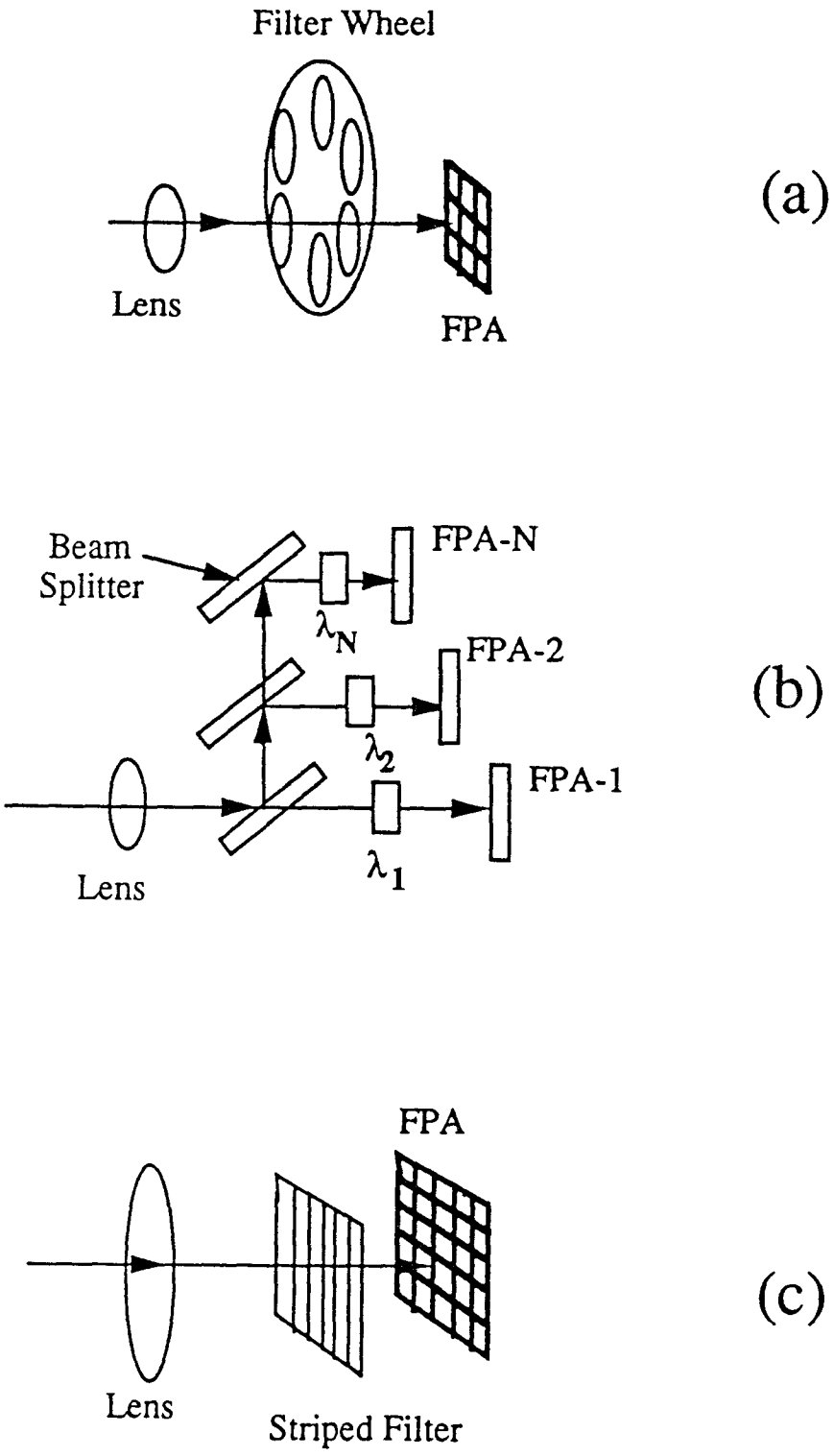

Figure 5 Choices of filter optics for the M-WIP system; Rotating filter wheel in (a), Beam-splitter in (b) and Striped filter in (c).

five wavelengths will have five detectors measuring radiation at five different wavelengths) does not change significantly. This approach, however, reduces the imaging resolution of the focal plane array by a factor determined by the number of wavelengths required.

The single chip IR camera with striped filter is the most compact and ultimately, the lowest cost system. The striped filter are not commercially available and several IR filter manufactures, to whom we had approached, were not interested in the development of such filters. Therefore, we have decided to fabricate the multi-wavelength narrow-band striped filters to be used with the 320 x 244 PtSi Schottky-barrier detectors IR-CCD imager at the David Sarnoff Research Center. The major focus of this thesis has been to design a photolithography mask for definition of such striped filters. The design considerations of this mask are presented in detail in next chapter.

2.4.2 320X244 PtSi SBD Imager based IR Camera System for M-WIP

The infrared camera system being developed for M-WIP application is based on a 320X244-element PtSi Schottky barrier detector array which is sensitive in 1 to 5μm spectral region. This imager has an interline (IT) readout architecture and was developed by David Sarnoff Research Center with the support of Rome Air Development Center.

The SBD FPA technology is described in detail by Kosonocky [6] and is briefly reviewed here. The operation of a back-illuminated PtSi Schottky-barrier infrared detector is illustrated in Figure 6. The infrared radiation with photon energy less than the bandgap of silicon (E_g =1.1 eV) is transmitted through the substrate. The absorption of the infrared radiation in the silicide layer results in the excitation of photocurrent across the Schottky-barrier (ψ_{ms}) by internal photoemission. The "hot" holes (those that have sufficient energy to go over the Schottky-barrier Ψ_{ms} formed between the silicide and the p-type silicon) are injected into the silicon substrate. Hence, a net negative charge will accumulate on the silicide electrode. Finally, the detection of the infrared optical signal is completed by transferring the negative charge from the silicide electrode into a CCD readout structure.

The spectral energy window of a back-illuminated Schottky-barrier detector is

$$\psi_{ms} < h\nu < Eg \tag{2-7}$$

where

ψ_{ms} - is the metal-semiconductor Schottky barrier;

$h\nu$ - is the photon energy; and

Eg- is the silicon bandgap energy (1.1 eV).

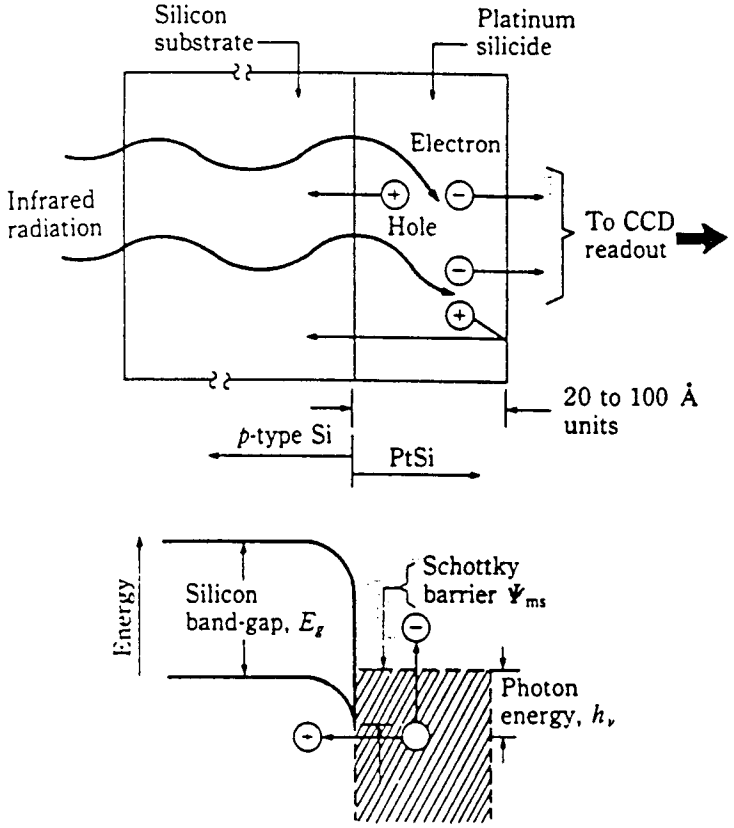

Figure 6 Operation of Schottky-barrier detector[6].

To achieve maximum responsivity in the MWIR band, the PtSi SBDs are usually constructed with an "optical cavity" (Al/Dielectric/Silicide film/Substrate/AR Coat). The responsivity, R of the Schottky-barrier detector can be approximated by a Fowler equation as

$$R = C_1\left(1-\frac{\Psi_{ms}\lambda}{1.24}\right)^2 \qquad (2\text{-}8)$$

where

R- is the responsivity in A/W;

C_1- is the quantum efficiency coefficient in eV^{-1};

Ψ_{ms} - is the metal-semiconductor Schottky barrier in eV; and

λ – is the wavelength of the infrared radiation in μm.

The measured spectral responsivity and quantum efficiency of the PtSi SBD array corresponding to C = 0.267 eV^{-1} and ψ_{ms} = 0.2272 eV is shown in Figure 7.

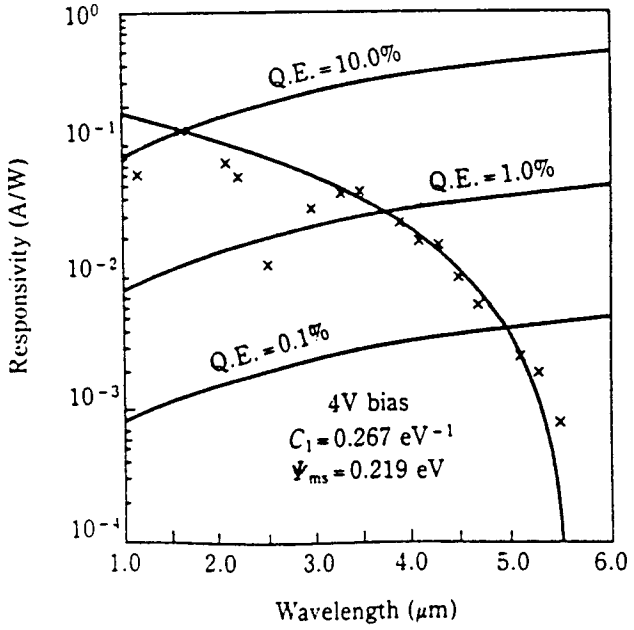

Figure 7 Measured spectral responsivity and quantum efficiency of the PtSi SBD array[6].

According to Eq. 2-8, the cut-off wavelength, λc, can be expressed as:

$$\lambda_c = \frac{1.24}{\psi_{ms}} \tag{2-9}$$

For typical PtSi SBDs with ψ_{ms} of 0.22 eV the value of λ_c is 5.7 μm.

The pixel layout for this FPA is shown in Figure 8. The total imager active area is 504 mil X 384 mil with a fill factor of 43%. The pixels are located on 40μm centers and the charge handling capacity of the imager is 1.4 x 10^6 electrons/pixel.

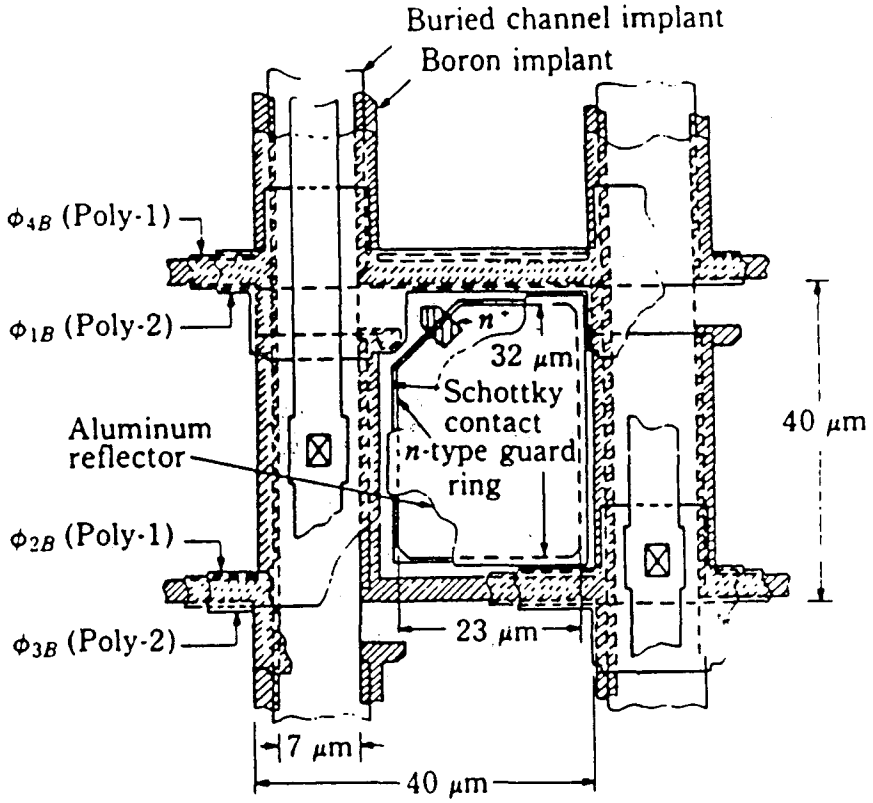

Figure 8 Pixel layout of the Sarnoff 320 X 244 FPA[6].

The interline transfer readout design of the imager is illustrated in Figure 9. As can be seen from the figure, two vertical detectors are interlaced in the same vertical CCD channel. The imager has 122 active lines per field, thus the standard NTSC video output is formed by a readout of a active imager video line followed by a blank video line [7]. In normal operation, the imager can be operated either in an interlaced (30 frames/s, 2 fields/frame) or an non-interlaced(60 frames/s, 1 field/frame) mode. The operation of two interlaced fields per frame is normally required to minimize flicker of the image. However, our application entails machine vision and field integration (non-interlaced operation) is the most efficient way to capture video data by a computer. Field integration involves operating the imager with one field (either half the pixels or combining two pixels) per frame with no blank lines inserted between active video lines. In addition, the imager can also be operated at different frame rates without needing to confirm to display standards for optimum radiometric operation.

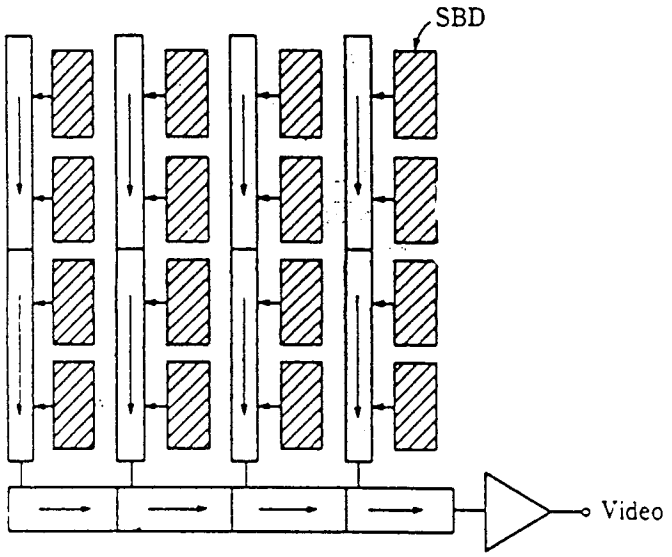

Figure 9 SBD FPA with vertically interlaced IT-CCD readout[6].

The electrical signal derived from photodetection is allowed to accumulate in the PtSi detectors for a specific charge integration time and then is transferred to the vertical CCD channels by a transfer pulse. The horizontal CCD channel then transfers the charge from the vertical CCD sequentially (320 pixels/line) line-by-line to the on-chip output amplifier to form the video output. The video output is digitized and then fed to DATACUBE Workstation for further signal processing and computation. It should be noted here that the M-WIP system is capable of automatic integration time control to avoid saturation of detectors. A detailed description of the operation of the camera operation can be found in the MS thesis of N. McCaffrey [8].

CHAPTER 3

MASK DESIGN FOR MULTI-WAVELENGTH STRIPED FILTERS

3.1 Introduction

The multi-wavelength imaging pyrometry technique requires measurements of radiation at multiple monochromatic (sufficiently narrow) spectral-bands. As discussed in the previous chapter, for very rapid processes such as RTP where the wafer temperature change can be as rapid as 100°/sec, it is very difficult to change wavelengths temporally. This problem of measuring temperature of a very rapidly changing process can be overcome by spatially detecting different wavelengths on the focal plane array.

In this chapter, an approach for achieving spatial detection of wavelengths by utilizing narrow-band multi-wavelength striped-filters in conjunction with the 320X244 element platinum silicide Schottky-barrier detector FPA is presented. Design issues related to defining striped filters are discussed and a complete mask design for investigating feasibility of three-wavelength striped filters is described.

3.2 Fabrication of Multi-Wavelength Narrow-Band Striped Filters

3.2.1 Approach

The PtSi detectors of the 320X244 element FPA, chosen for the Multi-Wavelength Imaging Pyrometer, are sensitive into 1-to 5-μm spectral range(see Figure 7 in Chapter 2). Thus, any number of narrow-spectral-bands can be selected within this spectral range for the M-WIP. One way to assign different spectral bands to various detectors is by using narrow-band optical filters. Since the each pixel in the FPA has 40μm center-to-center spacing (see Figure 8 in Chapter 2), the size of each filter should correspond to the pixel architecture. The best way to achieve this is by depositing and defining thin-film optical

filters directly on the FPA. However, the technology of defining small-geometry optical filters is not well developed. Alternatively, similar results may be achieved by depositing and defining filters on a transparent substrate which can be placed as close as possible to the FPA with proper alignment to the detectors. This chapter is mainly focused on the design of photolithographic masks for defining small geometry striped-filters on Si (polished on both sides) substrates.

3.2.2 Infrared Narrow-Band Filter Design

The narrow-band optical filters to be used for this approach has thin-film multilayer structure. Double cavity Fabry-Perot (single metal layer) and triple cavity Fabry-Perot (double metal layer) designs were considered for this application. The design of this optical filters was done by D. Hoffman (NJIT consultant). Detailed design and deposition technique for different optical filters is described by S. Amin, NJIT in his master's thesis [9]. A brief summary of optical thin-film design for fabrication of these filters is presented in this section.

The most basic design is a Dielectric-Spacer-Metal-Spacer-Dielectric (D-S-M-S-D) filter. Al_2O_3 or SiO_2 was chosen as dielectric, Al was chosen as metal, while Si was chosen as high refractive index (n) material in multilayer dielectric stack. The basic design of single wavelength "Fabry-Perot type D-S-M-S-D " filter is shown in Fig.10. A standard Fabry-Perot filter consists of a dielectric spacer bounded by two metal reflecting layers. Some broadening of the filter pass band can be achieved by stacking multiple filters to give a sequence Metal-Spacer-Metal-Spacer-Metal for a double half-wave filter. If the outer metal layers are replaced by dielectric stacks, absorption is reduced and transmission increased, yet long wave rejection is retained. The resulting D-S-M-S-D filter is called an induced transmission filter. The dielectric-spacer combination (D-S) acts as an antireflection system for the metal at the peak wavelength, thereby increasing its transmission.

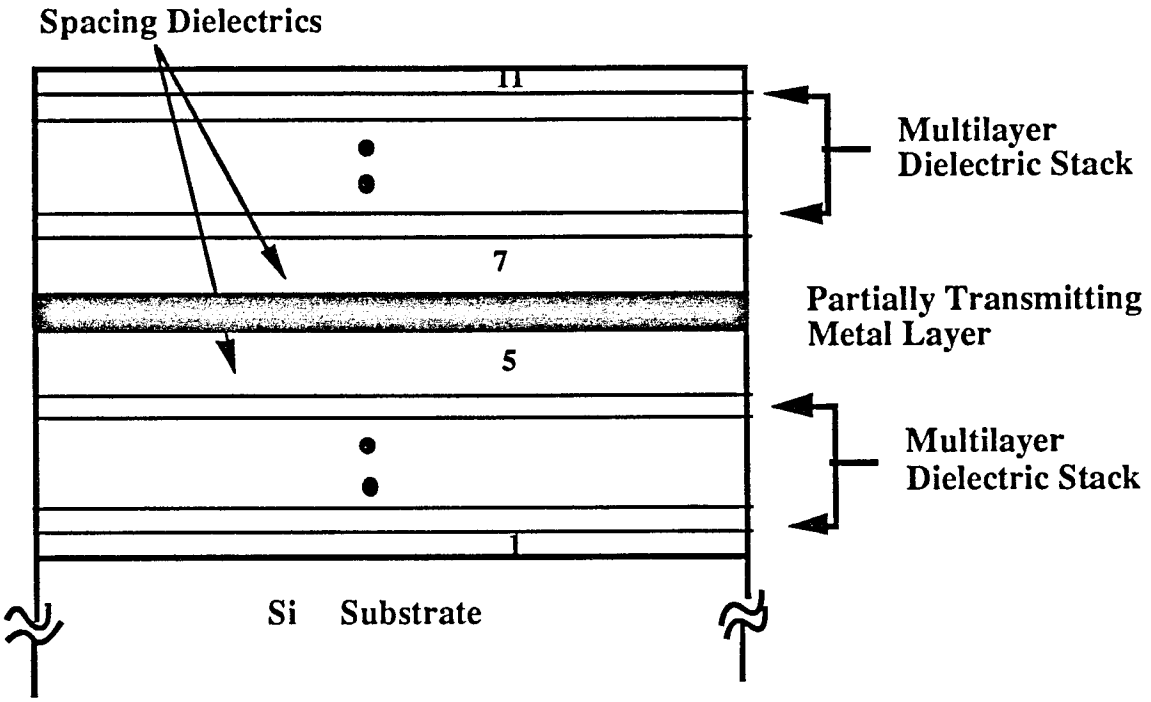

Filter Layers Details :

1 .25L 2 .25H 3 .25L 4 .25H
5 .488L
6 .03M
7 .488L
8 .25H 9 .25L 10 .25H 11 .125L

Where:
L : Al_2O_3 or SiO_2
H : Si
M :Al

.25L= a quarter wave thickness of low index material at design wavelength
.25H=a quarter wave thickness of high index material at design wavelength

Figure 10 Single wavelength D-S-M-S-D (Double Cavity Fabry-Perot) filter design with 11 layers.

To improve the rejection of the filter it is necessary to have two metal layers with a dielectric layer between them. This will provide rejection of the order of 0.0001% at the cost of somewhat reduced transmission. Transmission may also be reduced and the peak narrowed by increasing the thickness of the metal layer. In order to minimize the number of layers required in the antireflecting stacks, there should be a wide difference in the indices

of refraction of the alternating high and low index layers. The choice of Si and Al_2O_3 with indices of 3.65 and 1.55, respectively, will accomplish this.

3.2.3 Striped-Filter Fabrication Steps

For accurate determination of temperature of a colorbody using MWIP, it is required to have at least four-wavelength narrow-band filters [5]. However, it is also very important to have well-established fabrication technology available for definition of these filters. At present, the technology for defining these 11-15 layer filters in very small geometries (minimum 40μm center to center spacing with 10-20μm spacing between each wavelength filter) required for this application is not well established. For this reason, it was decided to define only three wavelength filters in a striped geometry in such a way that every fourth row or column of detectors will have the same wavelength assigned. The main objective for selecting only three wavelengths is to investigate some of the following critical issues:

(1) What is the minimum size of filters that can be defined?

(2) What is the best fabrication technology to achieve this?

(3) Should the filters be defined in horizontal or vertical stripes for optimizing the accuracy of the M-WIP?

For the fabrication of striped-filters, two basic approaches were considered. They are: (1) lift off approach, and (2) plasma etching approach. Figure 13 illustrates these two approaches.

In the lift-off technique (Figure 11a), the patterned resist film is formed first followed by a deposition of the multilayer filter. The filter will be deposited in both the open and covered areas. Dissolving away the resist will then "lifts off" the unwanted material deposited on the photoresist covered area. It should be noted here that the thickness of the photoresist film should be higher than that of the filter thickness. A disadvantage associated with this technique is a rounded feature profile.

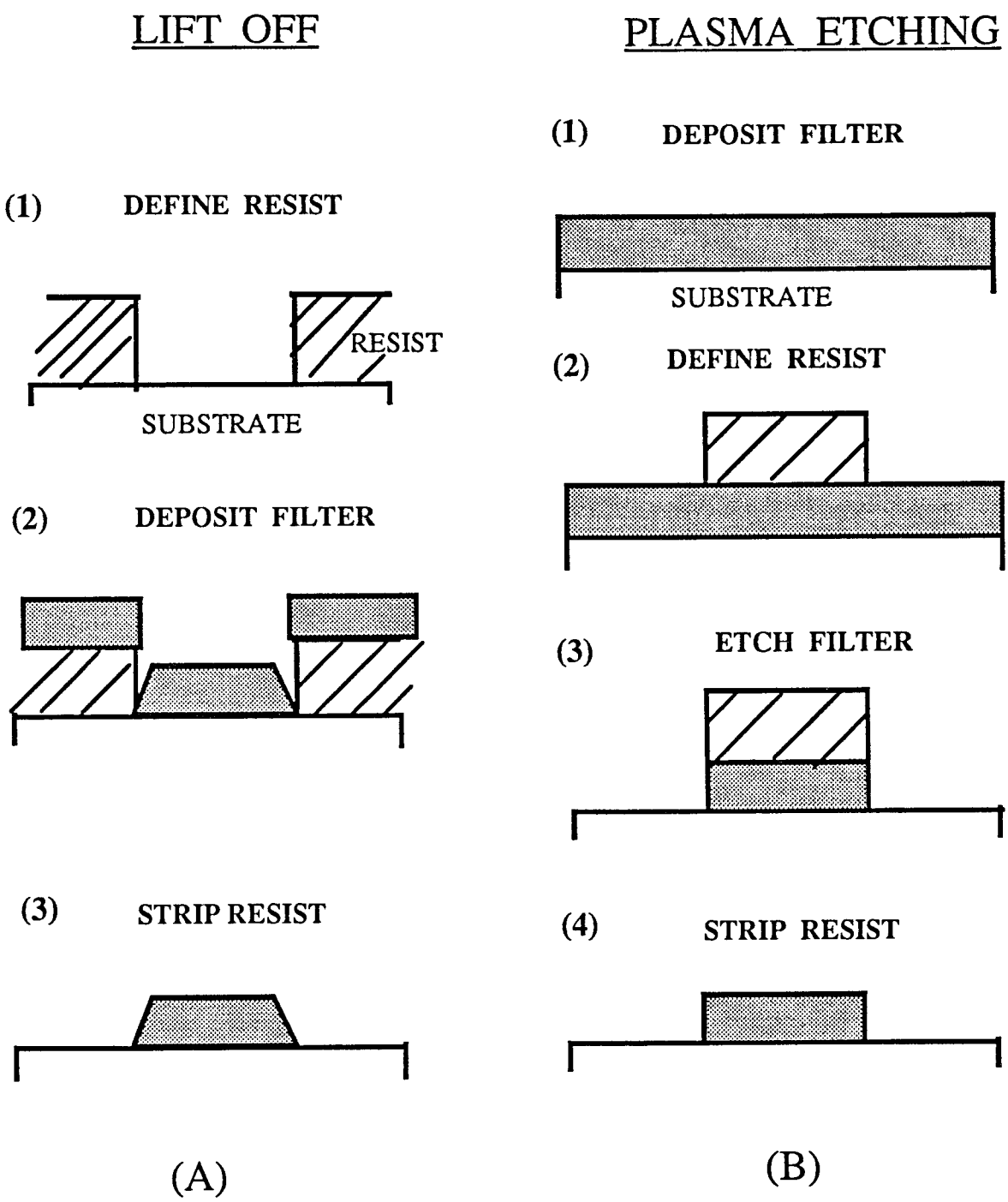

Figure 11 Schematic representation of two processing techniques for definition of striped-filters. (a) lift off technique and (b) plasma etching.

In plasma etching technique (Figure 11b), the filter is deposited on a bare substrate first followed by deposition and pattering of photoresist layer. The unwanted filter material is then plasma etched with the patterned photoresist layer acting as a mask.

Figure 12 shows a cross-sectional view of a three wavelength striped filter. For the fabrication of this filter, the following processing steps are required:

(1) Determine physical outline of the filters (i.e. separation between striped filters) by an opaque mask deposited on the silicon substrate using evaporated chromium metal.

(2) Using either plasma etching or lift-off technique, define filter λ_1.

(3) Repeat step 2 for definition of filters λ_2 and λ_3.

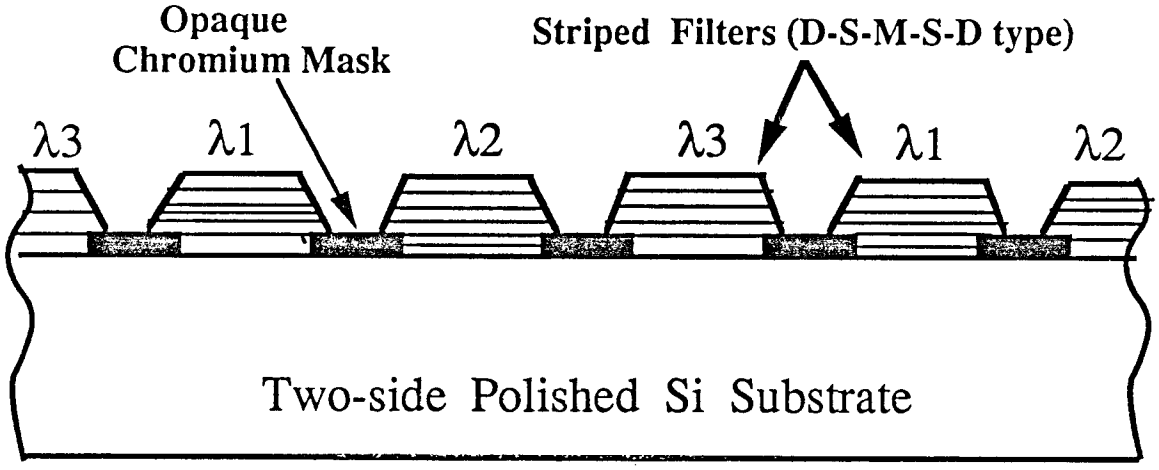

Figure 12 Cross-sectional view of a three wavelength striped filter

Definition of three-wavelength filters requires a four level photolithographic mask set. The first mask is for definition of opaque chromium layer and the other three masks are required for definition of each filter. To allow the flexibility for using either the plasma etching or the lift-off technique, a positive and a negative set of masks have been fabricated. The next section describes the four-level mask design in detail.

3.3 Mask Design

Using Mentor Graphics full custom IC layout editor, "ChipGraph", a four layer mask has been designed for defining various narrow-band striped filters on a 4-inch substrate. Since IR imager active area is only 12800 μm X 9760 μm, it is possible to include many striped-filter chips on a 4-inch substrate for the feasibility studies. The mask design presented in this chapter allows definition of twelve different categories of filters including two wave-length and three wave-length horizontal-striped and vertical-striped filters with various spacing in a single fabrication sequence. Filter dimensions were selected based on dimensions of the 320 x 244 Pt-Si SBD imager and the front head mounting assembly of M-WIP radiometer. Various test pads for optical characterization as well as Perkin-Elmer (PE) alignment keys and verniers for aligning individual layers during fabrication are also incorporated in the mask design.

3.3.1 Filter Dimensions

Exact filter dimensions were calculated based on Sarnoff 320 x 244 IR CCD focal plane array (FPA) dimensions. The imager has 320 pixels in the horizontal (H) direction and 244 pixels in the vertical (V) direction to allow standard NTSC format compatible video readout. The exact dimensions of the pixels and total imager area are shown in Figure 13 (for detailed layout of individual pixel, see Figure 8 in Chapter 2).The total imager active area is 12800 μm X 9760 μm. The pixels have dimensions of 23 μm (H) X 32 μm(V) and the separation between them 8 μm in vertical and 17μm in the horizontal directions. Two or three-wavelength striped filters can be defined either in vertical or horizontal direction in such a way that all of the detectors in each row or column will detect radiation at a specified wavelength.

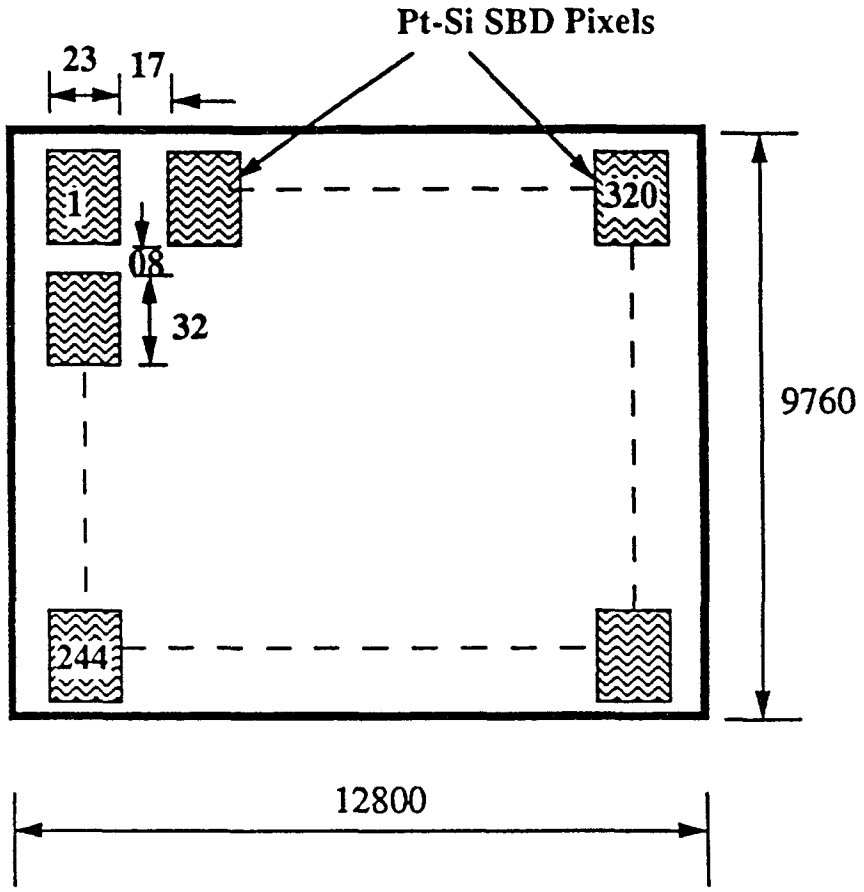

Figure 13 Dimensions of the 320 x 244 IR CCD FPA.

For defining one filter per raw requires minimum of 32 μm wide filters with 40μm center-to-center spacing while defining one filter per column requires minimum of 23 μm wide filters with 40μm center-to-center spacing. It appears from this requirements that fabrication of vertical striped filter should be less difficult. However, as discussed in Section 2.4.2, two vertical pixels are interlaced in the vertical CCD channel and only 122 lines are required for imaging. Thus, wider horizontal filters can be made (one filter covering maximum of two consecutive raw) without loosing the imaging resolution. For the case of vertical stripes, all 320 column detectors are used to form the image. Thus, from

processing point of view, vertical filters are more difficult to fabricate. Vertical filters can be made wider only at the cost of reduction in imager resolution.

3.3.2 Optical Considerations

Certain optical effects should also be considered for determination of filter dimensions so that cross-talk between pixels can be avoided. In other words, for achieving better temperature measurement accuracy, contribution of radiation on detected signal at each pixel from other than the specified wavelength should be minimized.

The general view of the striped filter positioned near 320x244 IR CCD imager in the M-WIP radiometer is shown in Figure 14. The back-side illuminated imager is mounted on a cold-finger inside the liquid N_2 dewar assembly. The striped filter will be placed as close as possible to the imager substrate as shown in Figure 14. To avoid unwanted radiation reaching the detector, a specially designed baffle assembly is used between the lens and imager. The geometry of the baffle was determined by N. McCaffrey using a program developed at the DSRC.

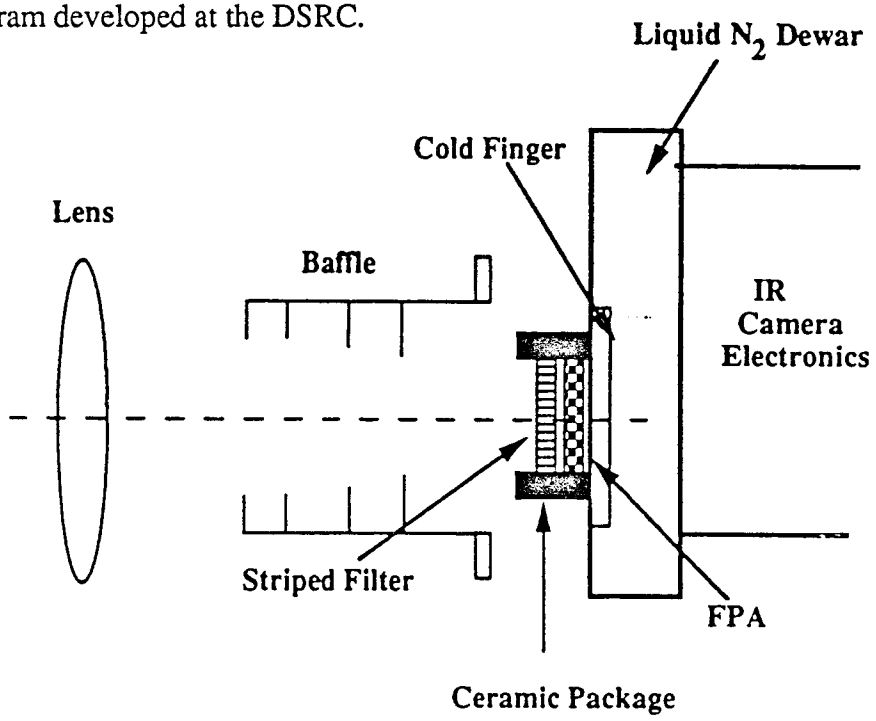

Figure 14 Striped filter position in M-WIP Radiometer.

Optical effects should also be considered during calculation of filter dimensions. These concepts were developed in collaboration with N. McCaffrey. Primary optical effect of filter distance from image plane on filter size is illustrated in Figure 15(a). As filter moves away from image plane (i.e. IR detector chip), minimum filter size become larger and the probability of cross-talk between pixels increases. Thus, filters should be placed as close as possible to the image plane. Figure 15(b) shows the optical arrangement for the M-WIP. Using baffle, detectors and ceramic package dimensions, the minimum filter size can be calculated using trigonometric formulas. In fact, these calculations will decide the maximum possible distance at which the filters can be placed for fixed filter dimensions. This optical requirement can also be fulfilled by using wider filter in combination with reduced imager resolution. Since the feasibility of minimum size of filters that can be fabricated is not known at present, detailed calculations were not made.

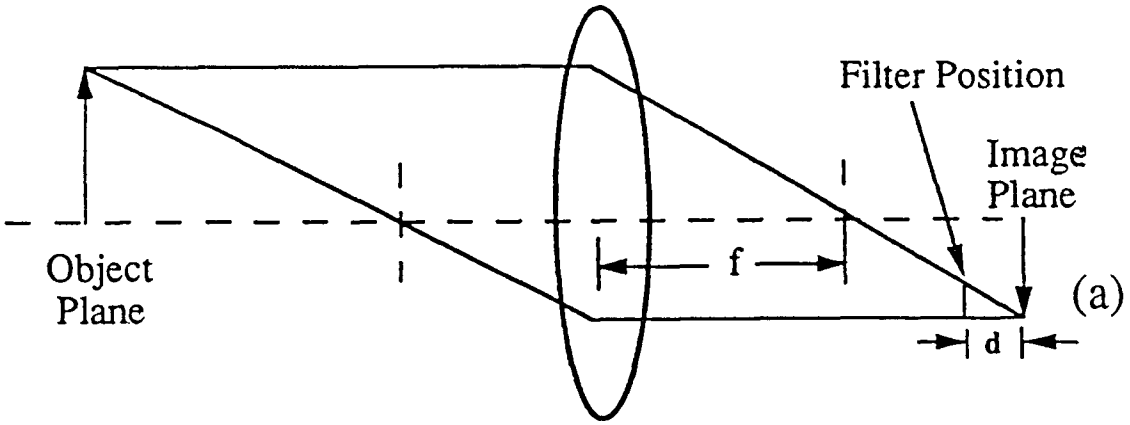

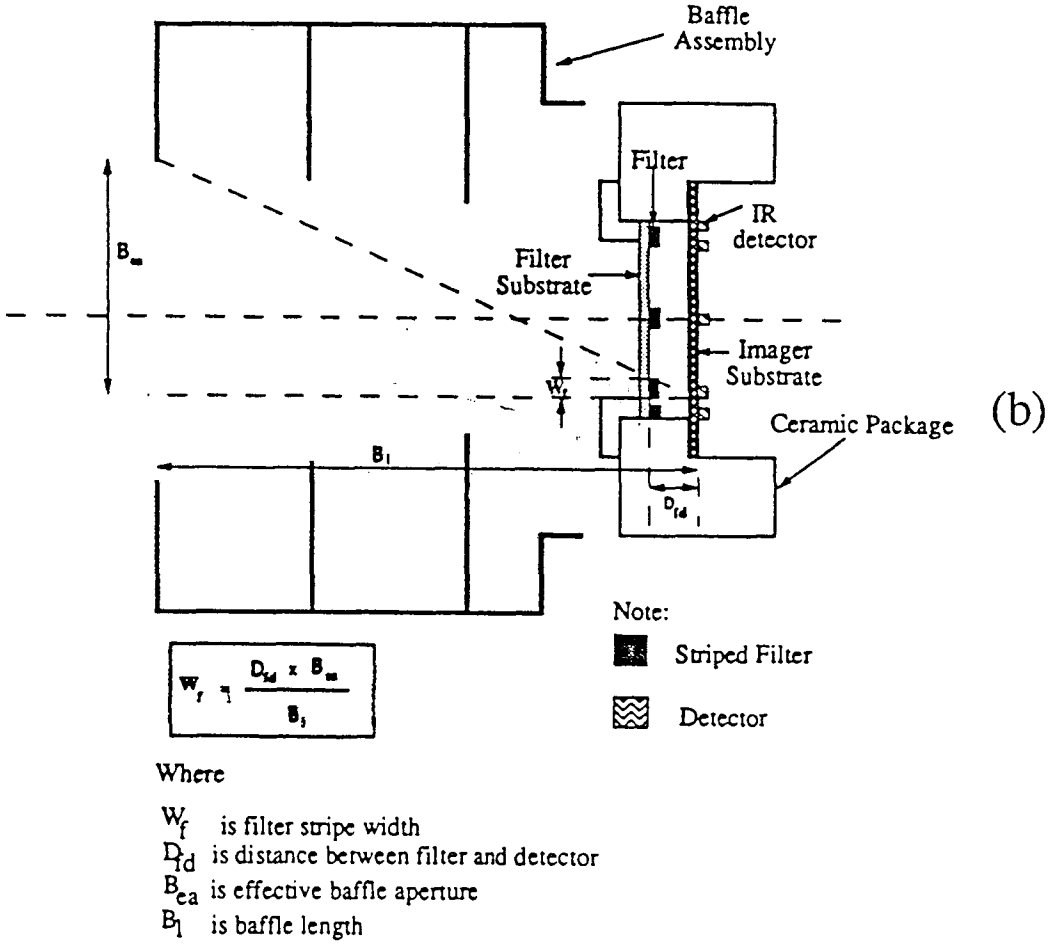

Figure 15 Effect of the distance between the filters and the imager on filter dimensions in (a) and (b).

It is known that refractive index is a function of wavelength [10]. As different wavelength rays pass through substrate, they refract with different angles. The effect of refraction on filter size is illustrated in Figure 16. However, the refractive indices of the substrate and thin films materials selected for filter fabrication are almost constant in 1μm to 5μm range. Hence, refraction effect can be neglected for our application.

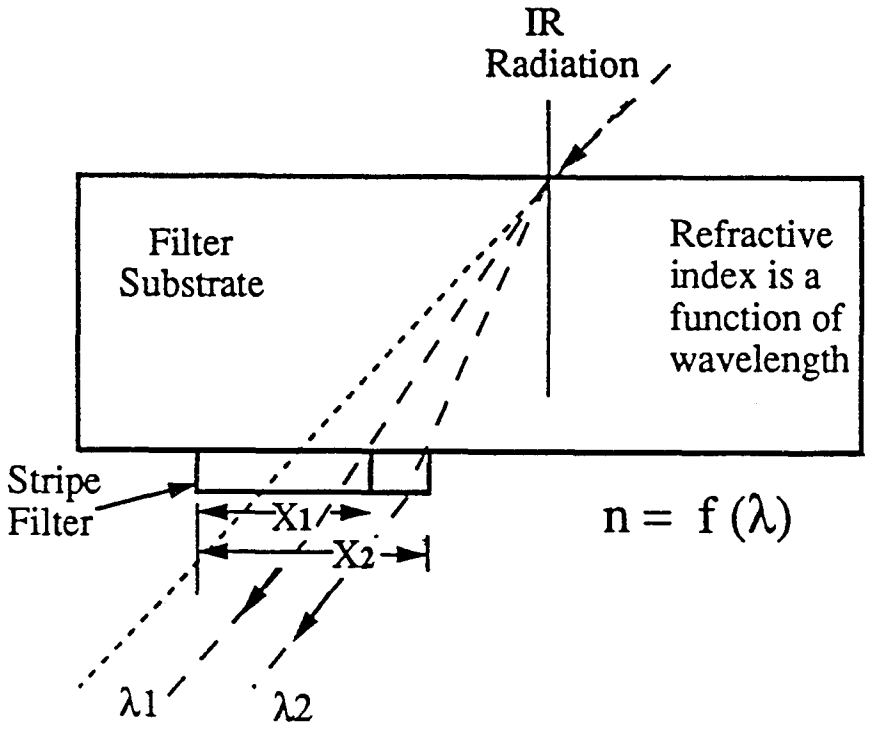

Figure 16 Effect of refraction on filter dimensions.

Dimensions of opening aperture also effect the minimum filter size required for perfect imaging. Diffraction limitation can be calculated using Eq. 4-1.

$$d_{diff} = 2.4\ \lambda\ f/\# \qquad (3\text{-}1)$$

Eqn. 3-1 relates the resolving power of the imager to the operating wavelength and the lens f/#. Using worst case analysis using the optics of the M-WIP, the filter size should be increased by approximately 9 μm due to diffraction effects.

3.3.3 Filter Categories

The final dimensions of the striped filters were decided after a number of discussions with Professor Kosonocky and consultations with Sarnoff staff [11]. As indicated previously, it was also decided to fabricate a positive and a negative set of masks for processing of stripes filters either by plasma etching or by the lift-off technique. Optical UV photolithography system at Sarnoff, having 1X projection and minimum resolution of 0.5 μm, will be used for striped filter fabrication. 4-inch wafers will be used for this study.

The IR imager active area is 12800 μm X 9760 μm and the area available for filter placement is 13843 μm X10160 μm (determined by the ceramic packaging of the imager). This allows 45 different filter chips to be produced on a single 4 inch wafer. Since the main objective of the mask design presented in this chapter was to allow a detailed feasibility study for fabrication of small-geometry striped filters, twelve different kind of filter geometries were chosen. Figure 17 illustrates the arrangement of 45 filter chips on a 4 inch wafer. Each filter-chip is separated by a 200μm wide scribe line and is identified by a legend. The dotted line in the figure represents the field allowed by Perkin Elmer Aligner.

Figure 18 categorically shows the variety of filter geometries which were included in the mask design. Various two and three-wavelength, horizontal and vertical, striped filter-chips with various stripe-widths were included in the mask design. Single-wavelength (with no stripes) filter chips were also included in the design to allow optical characterization of filters and assessment of uniformity of deposition across the 4-inch wafer. Alignment keys and verniers were also incorporated within four test chips for alignment of various mask layers. Each type of chips were identified in the design by a legend placed adjacent the active filter area. Specifications for each legend such as filter strip width, filter separation, chrome mask width, orientation (horizontal or vertical) and quantity are summarized in Table 1. It should be noted here that striped-filter geometries (T3 and T4) are included in the design for the purpose of defining very thin stripes of filters.

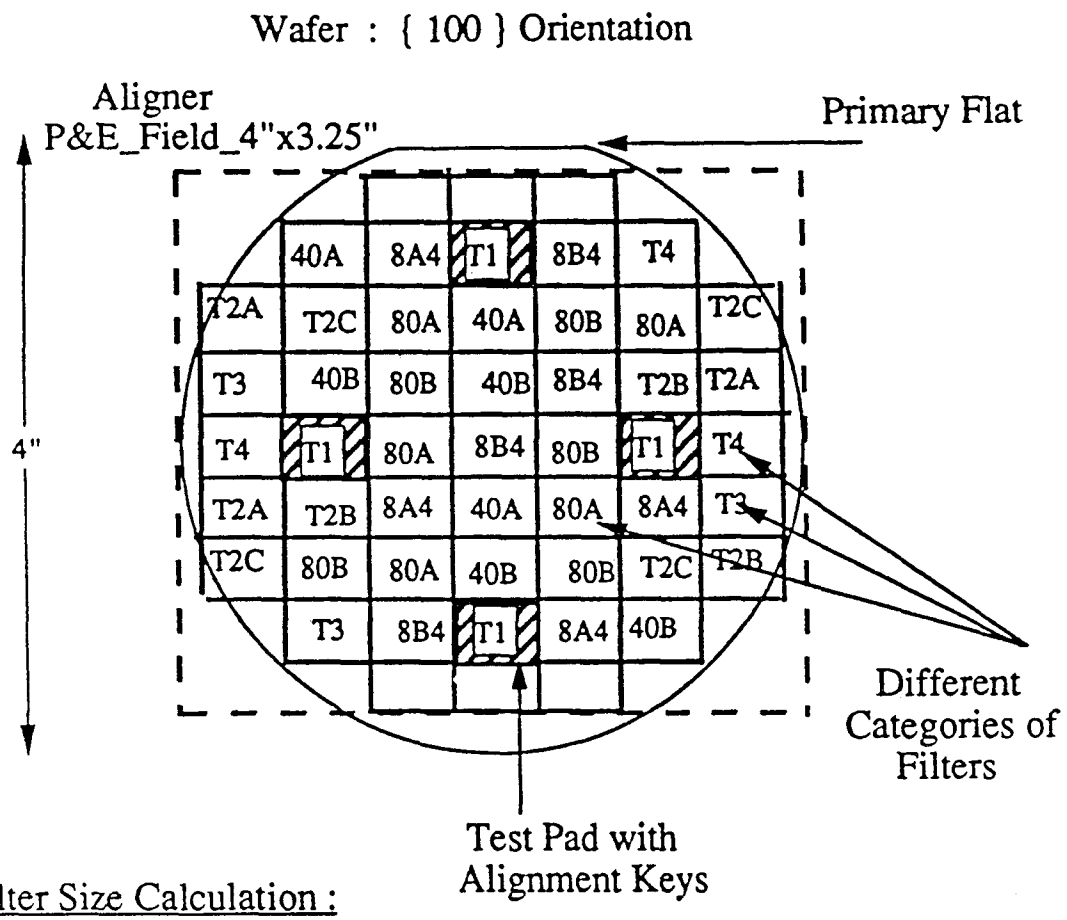

Filter Size Calculation :

(1) IR detector chip active area = 12 800 μm x 9760 μm

(2) Filter active area (including notation) = 13100 μm x 9860 μm

(3) Scribe line width between two filter chips = 200 μm

(4) Final filter size (after cutting) = 13300 μm x 10060 μm

(5) Area available for filter placement = 13843 μm x 10160 μm
or 0.545" x 0.4"

Figure 17 Illustration of the filters pattern to be processed on a 4-inch Si wafer.

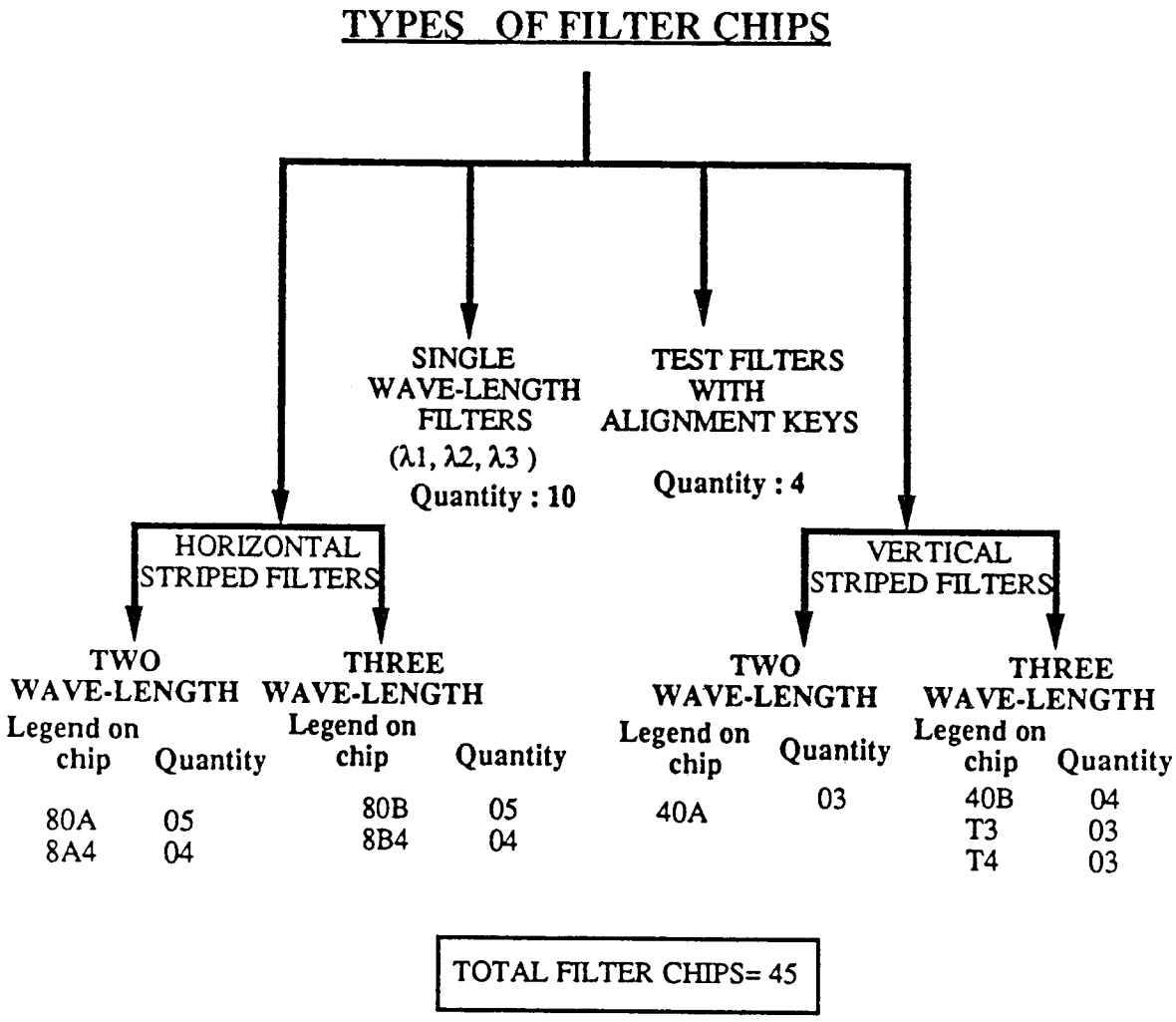

Figure 18 Different categories of filter-chips on a 4 inch substrate.

For easy understanding of Table 1, schematic of filter 80A is illustrated in Figure 19 as an example.

Table 1 Summary of striped filters categories.

Sr. No	Filter Chip Legend	Type V / H/N	Wave-length 2 or 3	Dimensions (μm)				Over lap (o)	Quantity (No)
				Filter strip		Chrome strip			
				Width (w)	Separ. (s)	Width	Separ.		
STRIPED FILTER CHIPS									
1	40A	V	2	33	07	17	23	05	03
2	40B	V	3						04
3	80A	H	2	70	10	30	50	10	05
4	80B	H	3						05
5	8A4	H	2	60	20	40	40	10	04
6	8B4	H	3						04
TEST FILTER CHIPS									
7	T1	V	3 + align.marks	2540	1500	1500	2500	20	04
8	T2A	N	λ1	12800	-	-	-	-	03
9	T2B	N	λ2						03
10	T2C	N	λ3						04
11	T3	V	3	25	05	15	15	05	03
12	T4	V	3	14	06	10	10	02	03

Note: V: Vertical Stripes,
H: Horizontal Stripes,
N: No Stripes

TOTAL NO. OF CHIPS = 45

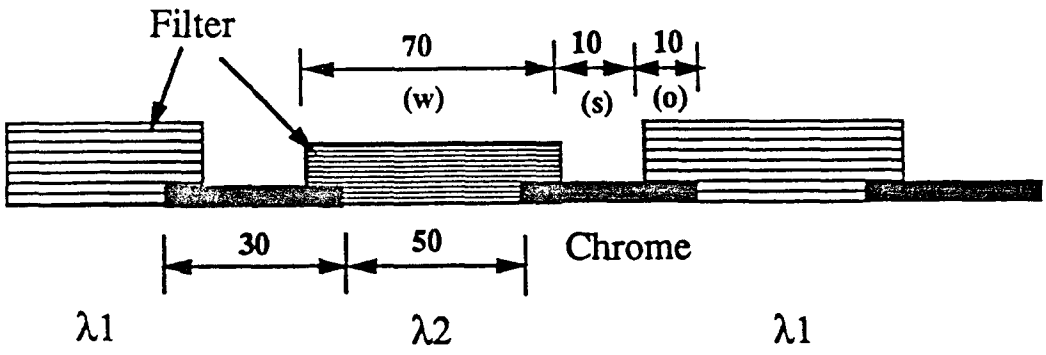

Note :

W is the filter stripe width in μm
S is the separation between two filter stripes in μm
O is the overlap of filter stripe and chrome stripe in μm

Figure 19 Schematic view of filter-chip (80A) with important dimensions.

3.4 Mask Layout

3.4.1 Layout Editor

Mentor Graphics full-custom IC layout editor, "ChipGraph " was used for layout of mask design [12] on HP Apollo workstation. ChipGraph^{TM} is a graphics editor that supports the physical layout of full custom integrated circuits. A four layer process definition file was created in the ChipGraph database. The process definition file (PDF) sets the layers for use during the edit session and the kinds of objects that can be placed on the defined layers. The object classes, that ChipGraph allows to create, are shapes, paths, instances, perimeters, ports, arrays of instances, and stretchable elements. ChipGraph is an editor that comes with conversion programs to read or create both GDSII^{TM} and CIF formats of the layout for transferring the layout design to mask manufacturer. TRANSLATE program was

used to convert ChipGraph database into GDSII stream format data according the specifications supplied by the mask manufacturer.

3.4.2 Filter Layout

As explained in section 3.3.3, there are 12 different types of filters with the total of 45 filter chips were designed on a 4 inch wafer. Initially, layout was made for basic 12 types of filters and then was repeated at several places on a wafer (see Figure 17, Section 3.3.3). Binary process definition file was created for the four mask layers. These mask layers are: "Chrome_1", "Lambda1_2", "Lambda2_3" and "Lambda3_4". The first layer mask "Chrome_1" is for defining opaque chromium layer while the second layer mask "Lambda1_2" is for defining filter at wavelength λ_1. Similarly, third and forth layer masks "Lambda2_3" and "Lambda3_4" are for defining filters at wavelengths λ_2 and λ_3, respectively.

The detailed layout of the filter-chip 80A (two-wavelength horizontal striped-filter with 80μ center to center spacing) is shown in Figure 20. The legend identification of the chip is clearly visible in this layout. It should be noted here that this layout consists of only four layers (with patterns). The rest of the layers (without patterns) shown on the right hand side of the figure are for representing the external boundary and are not useful for present design. Layouts for other types of striped filter-chips are presented in Appendix A.

The layout of a test-filter chip (T1) is shown in Figure 21. The layout of this filter-chip allows optical characterization of three wavelength-filter on the same chip. Perkin Elmer alignment keys and verniers were also incorporated in this chip. Specifications for alignment keys were provided by L. White of the David Sarnoff Research Center.

The verniers are useful for determination of horizontal and vertical mismatch between layers in positive and negative directions. The verniers for first and second layers are shown in Figure 22. Critical dimensions check patterns of the sizes of 2μm, 5μm and 7μm have also been placed below vernier patterns for characterization of the fabrication

process. Various single-wavelength (with no stripes) filter chips were also included in the mask design to allow optical characterization and assessment of uniformity of deposition across the 4-inch wafer.

The complete mask design with all four layers is shown in Figure 23.

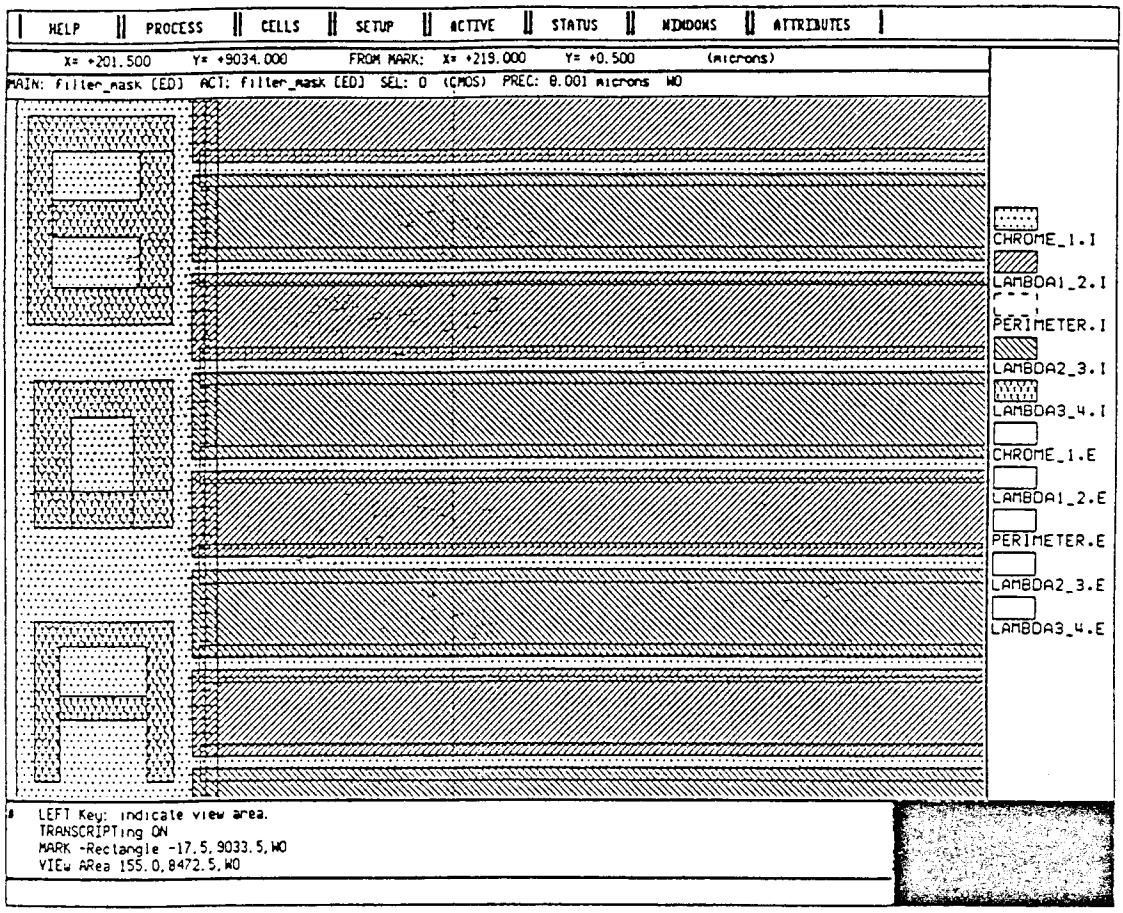

Filter 80A

Filter strip width = 70 μm; Separation between stripes= 10μm

Chrome width = 30 μm; Separation between stripes= 50μm

Overlap between chrome strip and filter stripes= 10μm

Figure 20 Layout of a three-wavelength horizontal striped filter (80A).

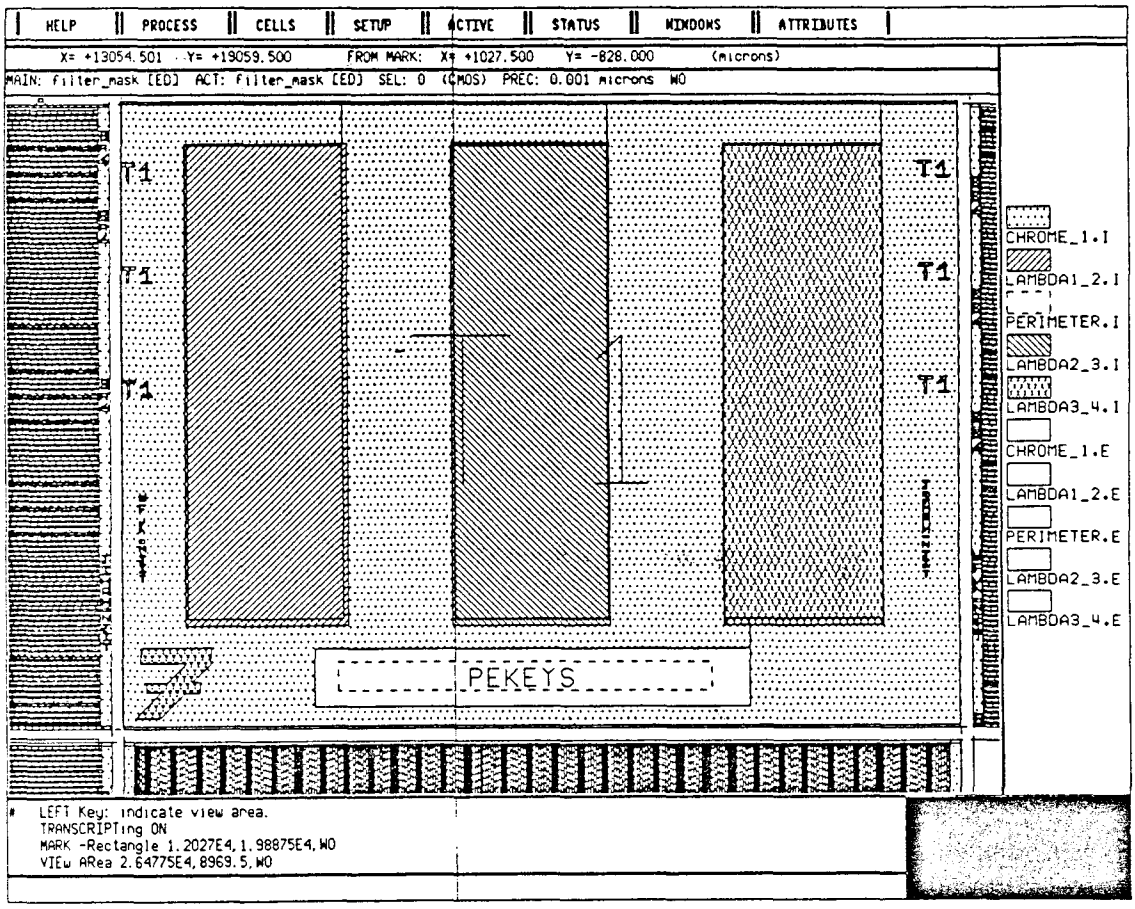

Figure 21 Basic test filter-chip includes all three-wavelength filter. Alignment keys are placed at the bottom of the test filter.

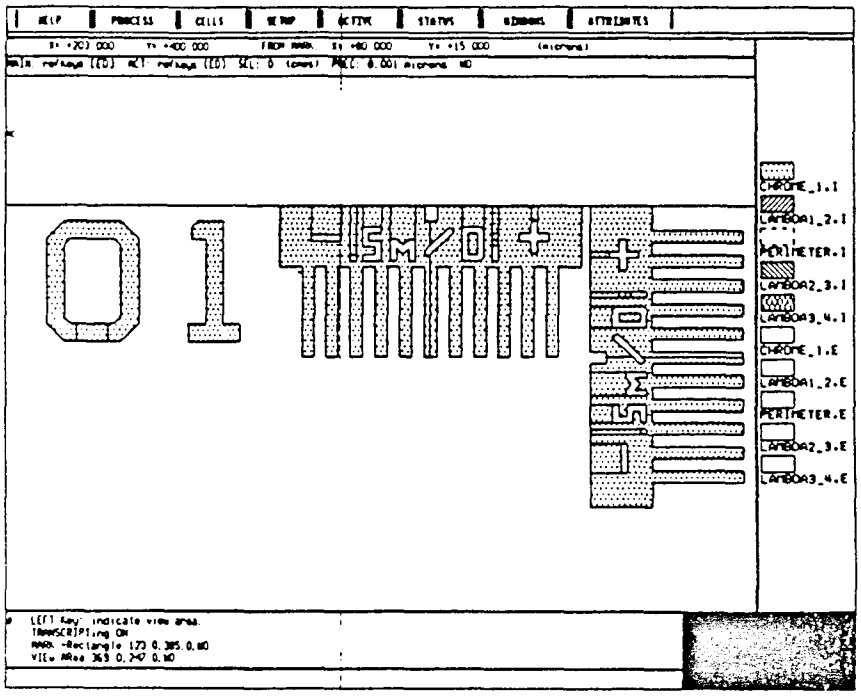

(a)

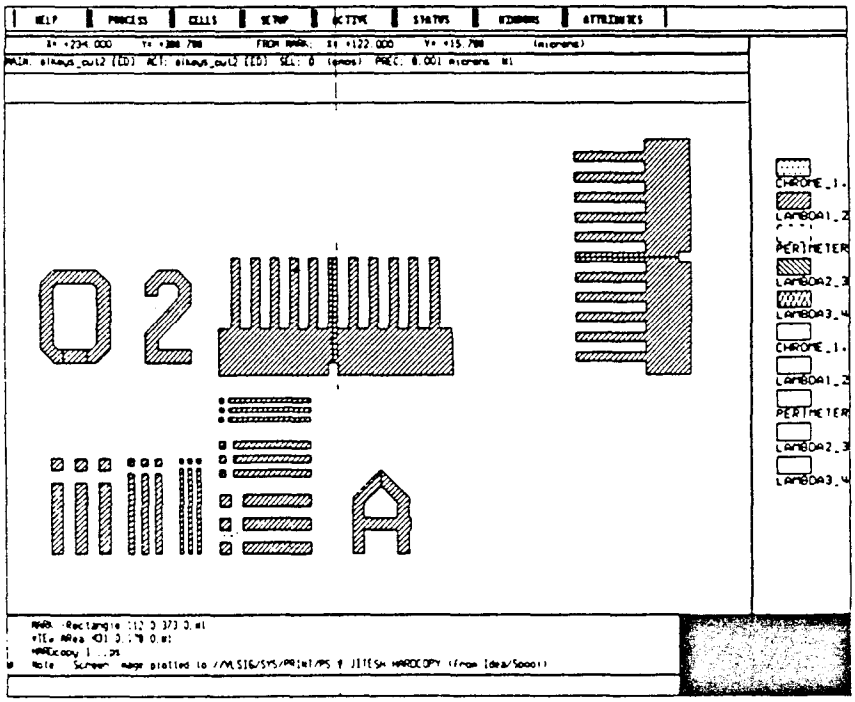

(b)

Figure 22 Layout for vernier for first (reference) layer in (a) and second layer vernier and basic critical dimensions (CD) pattern in (b).

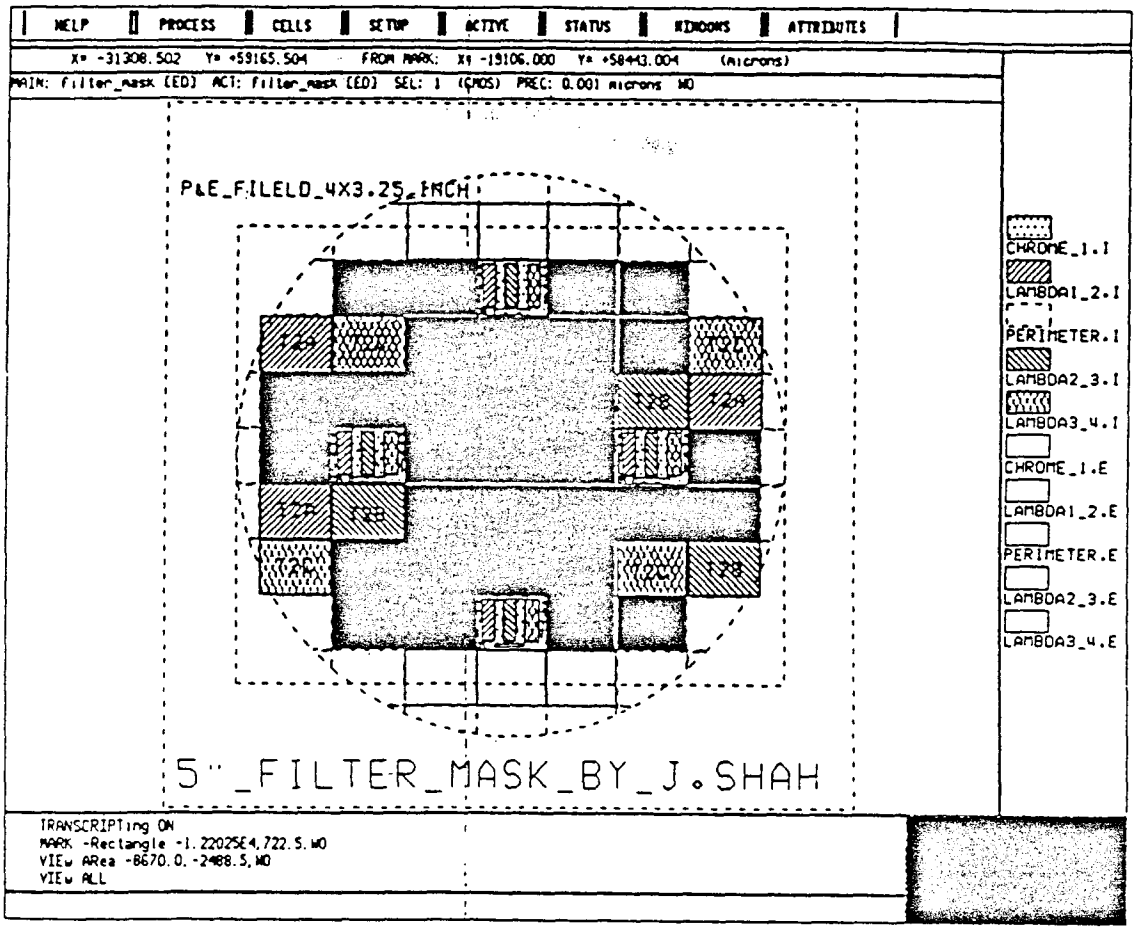

Figure 23 Complete schematic for 5" filter mask including all filters (Total Nos. : 45) on 4" Si wafer.

3.5 Mask Specifications

For fabrication of narrow-band striped-filters on 4" Si wafer, a four layer 5" mask was designed and fabricated at MICROMASK,Inc., as a part of this thesis. Both positive and negative sets of masks were obtained.

The 1X CORE/MEBES generated masks have the following specifications.

(i)	Material Type:	LR Chrome LEU
(ii)	Size:	5 X 5 X 0.090 inch
(iii)	Address Size:	0.50μm
(iv)	Minimum Feature Size:	2.0 μm
(v)	Critical Dimension	Tolerance: ± 0.20μm
		Uniformity: 0.20μm
(vi)	Defect Size:	1.5μm
(vii)	Defect Density:	1 defect/square inch
(viii)	Array Registration:	±0.25 μm
(ix)	Mask Field:	Clear (for plasma etching)
		Dark (for lift-off technique)
(x)	Digitized Area:	Dark (for plasma etching)
		Clear (for lift-off technique)

Using these masks, striped-filters will be fabricated at the David Sarnoff Research Center, Princeton, NJ. under direct supervision of Dr. B. Singh and Dr. L. White. Optical characterization tests of samples filters including Fourier Transform Infrared Spectroscopy (FTIR)will be performed by Luis Casas at EPSD, U.S. Army, Fort Monmouth, NJ.

CHAPTER 4

EMISSIVITY MODELING OF THIN-FILM MULTI-LAYER STRUCTURES

4.1 Introduction

Since least-square based curve-fitting technique requires an emissivity model (see Chapter 2, Section 2.3.3) as an input, prior knowledge of emissivity is useful for optimization of the Multi-Wavelength Imaging Pyrometer (M-WIP). In semiconductor processing, thin films are being etched or deposited on a variety of substrates and the emissivity of the multilayer structures changes continuously. Therefore, modeling of spectral emissivity of thin film multilayer structures is useful for selection of the emissivity model, the spectral range and number of required wavelengths for the M-WIP system. It is also important to know the directional behavior of emissivity for various material systems due to the fact that detection of radiation emitted in the normal direction is not possible in many processing equipment. Furthermore, it is also possible to determine *in situ* the film thickness and uniformity of etching or deposition using M-WIP if the emissivity as function of thickness of the multi-layer structure is known. For plasma etching application, end-point of etching can also be determined by monitoring change of emissivity at the interface.

In this chapter, a simple model to calculate emissivity of a multilayer structure is presented after describing the fundamentals of emissivity. Then, simulation results of emissivity modeling of various multilayer thin film structures, commonly used in plasma etching, are presented and discussed. It should be noted here that the model presented in this chapter can also be applied to other processing techniques such as evaporation, sputtering, CVD and RTP.

4.2 Fundamentals of Emissivity

Emission of radiation from a material is a volumetric process and is strongly dependent on the optical and surface properties of the material. In other words, only a portion of the radiant flux generated within the material may be emitted. For a strongly absorbing materials, such as metals, only a few micron thick material may contribute to the emitted radiation. For semitransparent materials, the entire volume of the material may contribute to the total emitted radiation. Emissivity also depends on emittance angle, wavelength and temperature due to the fact that optical properties of any material are dependent on these parameters [13].

Basically, emissivity is a measure of the relative response of a radiator with respect to a blackbody. For a perfect blackbody emissivity (ε) is always unity. A graybody is defined as a radiating body whose emissivity is less than unity and is independent of wavelength. For a colorbody (real-body), emissivity is a function of wavelength, temperature and angle of emittance. Figure 24 illustrates spectral and directional distribution of emitted radiation from a blackbody and a real-body [2]. It is important to note that emissivity may assume different values according to whether one is interested in emission at a given wavelength, in a given direction or in weighted averages over all possible wavelengths and directions.

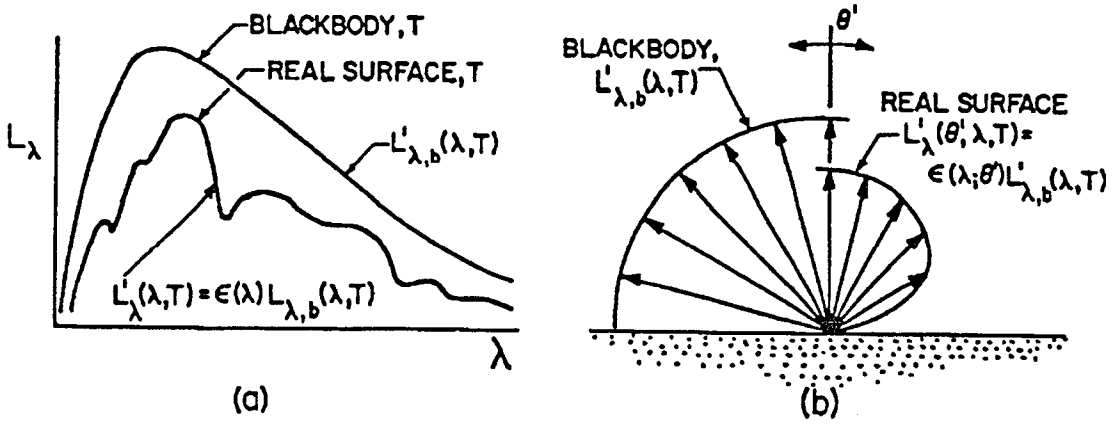

Figure 24 Comparison of blackbody and real body emission (a) spectral distribution and (b) directional distribution of radiance.

The spectral radiance, $L_{\lambda,em}$, is defined as the radiant flux (Φ_{em}) emitted at the wavelength λ in a given direction per unit emitting surface area normal to this direction, per unit solid angle about this direction, and per unit wavelength interval $d\lambda$ about λ. The spectral radiance, which has the units of $[W / m^2 \cdot sr \cdot \mu m]$, may then be expressed as

$$L_{\lambda,em}(\lambda,\theta) = \frac{d^3\Phi_{em}}{dA_n d\omega\, d\lambda} \tag{4-1}$$

Radiant power per unit area of the emitting surface can be determined by integration of Equation (4-1) over finite solid angle and wavelength interval, provided the spectral and directional distributions of the spectral radiance are known.

Emissivity, in general, is defined as a ratio of the radiation emitted by a real-surface to that by a blackbody. The spectral-directional emissivity $\varepsilon(\lambda,\theta,\phi,T)$ of a surface at temperature T is defined as the ratio of radiance emitted at wavelength λ and in the direction of (θ, ϕ) to the radiance emitted by a blackbody at the same temperature and wavelength

$$\varepsilon(\lambda,\theta,\phi,T) = \frac{L_{\lambda,em}(\lambda,\theta,\phi,T)}{L_{\lambda,b}(\lambda,T)} \tag{4-2}$$

As a practical matter, optically homogeneous materials with smooth surface are usually isotropic in azimuth, and hence the ϕ direction need not be specified.

The emissivity factor is used to scale radiometric equations that use blackbody models. When dealing with real-bodies, it is necessary to insert the emissivity factor (ε) into the blackbody equations. Similarly Planck's law (Eq. 2-1), the Stefan-Boltzmann law (Eq. 2-2), and the Wien displacement law (Eq. 2-3) should be modified by multiplying the right-hand term by the appropriate value of ε.

4.3 Basic Emissivity Model for Thin-Film Multilayer Structures

Emissivity can also be derived from the Kirchhoff's law by considering an object in an isothermal cavity. If there is a temperature difference between the object and the cavity, there will be heat transfer. If the object absorbs a portion α of the input exitance E (W/m^2) that a blackbody would emit at that temperature, then the object will emit an amount εM equal to that absorbed; that is,

$$\alpha = \varepsilon \tag{4-3}$$

where

α– is the absorptance; and

ε– is the emittance.

This is an expression of Kirchhoff's law, which states that the absorptivity α of a surface is exactly equal to the emissivity ε of that surface [14]. Also, radiation incident on a substance can be transmitted, reflected (or scattered) and absorbed. Conservation of energy requires that

$$\alpha + \rho + \tau = I \tag{4-4}$$

where

ρ– is the reflectance; and

τ– is the transmittance.

Kirchoff's law can also be used to determine emissivity of a multilayer structure. Emissivity of a multi-layer structure is described in detail by Vipul Patel in his Ph.D. thesis and is briefly reviewed here [15]. The simplest case for understanding the basic concepts of emission from a multi-layer thin-film structure is the case of a semitransparent slab with parallel-surfaces. Emission from a semitransparent slab with parallel surfaces was first described by McMahon [13].

For a slab of total thickness(d) with optical properties n(λ,T) and k(λ,T), he showed that the emissivity can be expressed as

$$\varepsilon(\lambda,T)=\frac{\{1-r(\lambda,T)\}\{1-t(\lambda,T)\}}{1-r(\lambda,T)t(\lambda,T)} \tag{4-5}$$

where

$t=\exp\left(\frac{4\pi kd}{\lambda}\right)$-is the internal transmission; and

$r=\left(\frac{\bar{n}-1}{\bar{n}+1}\right)^2$-is the reflectivity in which $\bar{n}$ is the complex index of refraction.

It is important to recognize that this reflectivity, r, is based upon single reflection. He also showed that Kirchhoff's law can be applied to the semitransparent slab in the form of:

$$\varepsilon(\lambda,T)=1-\rho(\lambda,T)-\tau(\lambda,T) \tag{4-6}$$

where

$\rho(\lambda,T)=r\left[1+\frac{t^2(1-r)^2}{1-r^2t^2}\right]$ and $\tau(\lambda,T)=t\left[\frac{(1-r)^2}{1-r^2t^2}\right]$ are the apparent reflectivity and transmittivity and includes multiple reflections.

Gardon extended the theory of McMahon and considered the diffuse character of the generated radiant flux, rather than only the unidirectional normal case, so that the hemispherical and directional emitted fluxes can be determined [16, 17]. He treated the flux generated as unpolarized and included the directional dependence of plane parallel and plane perpendicular polarization components. Some of the useful emissivity concepts developed based on his work are briefly summarized here.

Gordan treated the radiation generated within material to be unpolarized and assumed that the energy in p- and s-polarized components are equal. The processes of

reflection and refraction determine the fraction of primary radiation, generated within the material, which appears as emitted radiation. A fraction, r (known as Fresnel reflection coefficient), of the directional intensity incident on the surface will be reflected. The well-known Fresnel relation in its elementary form is

$$r = \frac{1}{2}(r_p + r_s) \tag{4-7}$$

where

$$r_p = \left[\frac{n_1 \cos\theta_i - n_2 \cos\theta_r}{n_1 \cos\theta_i + n_2 \cos\theta_r}\right]^2 \quad \text{and} \quad r_s = \left[\frac{n_2 \cos\theta_i - n_1 \cos\theta_r}{n_2 \cos\theta_i + n_1 \cos\theta_r}\right]^2$$

r- is the reflectance of the interface for unpolarized incident flux;

θ_i- is the incidence angle;

θ_r- is the refracted angle;

r_S- is the reflectance for radiation polarized in a plane $\perp$ar to the plane of incidence (known as S-polarization);

r_P- is the reflectance for radiation polarized in a plane $\parallel$ to plane of incidence (known as P-polarization);

n_1- is the refractive index of medium 1; and

n_2- is the refractive index of medium 2.

The fraction (1-r) is then refracted into second medium according to Snell's law.

$$n_1 \sin\theta_i = n_2 \sin\theta_r \tag{4-8}$$

For an opaque material, emissivity can simply be represented as 1-ρ. When the material has appreciable absorption, the complex index of refraction must be used. Thus, it is expected that metals and dielectrics should have different emissive properties. Also due to polarization effects, the directional dependence of emissivity is drastically different for metallic and dielectric materials.

The angular dependency of the directional emissivity for selected values of optical properties using the Fresnel Relation (Eq. 4-7) is illustrated in Figure 25. The directional

behavior of emissivity for dielectric materials is plotted on the right-half of this figure. Dielectric materials with lower n value display higher emissivity values. Emissivity of dielectric materials is independent of direction up to approximately 45°-55° and then falls off with increasing angle. In contrast, metallic materials (plotted in left-half of the figure) have lower values of normal emissivity which increases with angle followed by a sharp decreases above a critical angle. The value of this critical angle is dependent on n and k. It is evident from this figure that metallic materials are better emitters at high emittance angles.

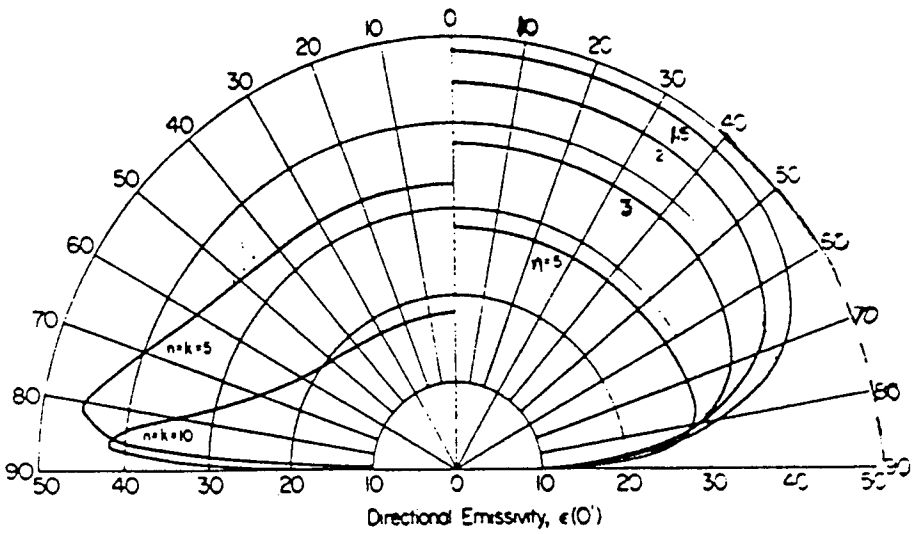

Figure25 The directional emissivity as a function of index of refraction, n, for nonmetallic materials (k=0) and for metallic materials with n=k.

The emissivity model given by Eq. 4-6 can be applied to the practical application of thin film processing where thin films are present on a semitransparent substrate. However, the interference occurring from the coherent reflections from thin film interfaces and the polarization effects should be included in the model. Figure 26 graphically illustrates the basic concept of emissivity for a multilayer structure. If the optical properties of the films and the substrate are known, emissivity of any multilayer structure can be determined by calculating apparent reflectivity and transmittivity using thin film optical analysis. A detailed account on thin film optical analysis is given in the book by H. Macleod [18].

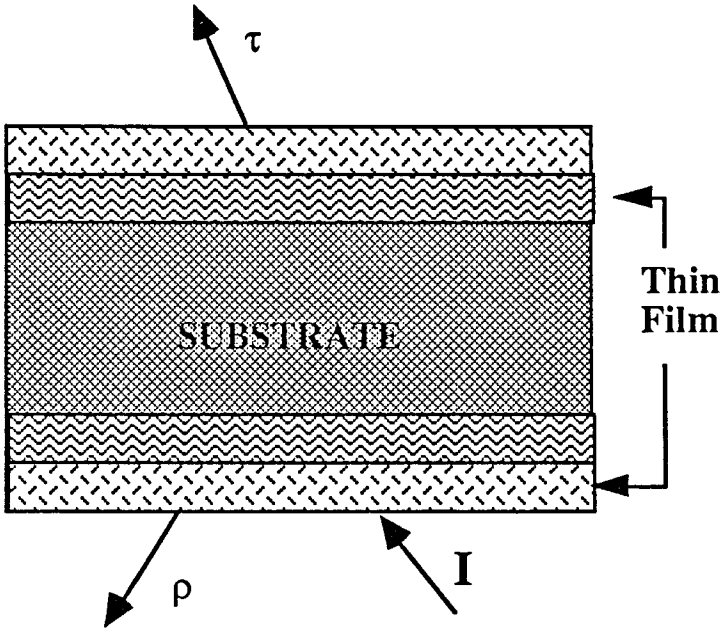

$$\rho + \tau + \alpha = I$$

$$\varepsilon \text{ (Emissivity)} = \alpha \text{ (Absorptivity)}$$

$$\varepsilon = I - \rho \text{ (apparent reflectivity)} - \tau \text{ (apparent transmittivity)}$$

Figure 26 A basic emissivity model for a thin-film multilayer structure.

4.4 Simulation Results and Discussion

The model described in the previous section was used to determine emissivity of various thin-film multi-layer structures, commonly used in plasma etching, as a function of thickness being etched. The following structures were studied.

(1) Poly-Si (5000Å)/SiO_2 (5400Å)/Si substrate(0.5 mm)/SiO_2 (5400Å)/Poly-Si (5000Å);

(2) Poly-Si (5000Å)/SiO_2 (5400Å)/Si substrate;

(3) Poly-Si (5000Å)/SiO_2 (200Å)/Si substrate;

(4) $TaSi_2$ (5000Å)/SiO_2 (3000Å)/Si substrate; and

(5) $TaSi_2$ (1000Å)/Poly-Si (4000Å)/SiO_2 (200Å)/Si substrate.

Film*Star thin film evaluation software package was used for this modeling work. Published optical constants (at 300K) of the materials of interest (Si, SiO_2, Poly-Si and $TaSi_2$) were used within spectral range of 2.5 μm to 5.0 μm [19, 20]. As optical constants are intrinsic properties of materials, it do not vary with thickness of materials. Optical constants for polycrystalline silicon (Poly-Si) with doping concentration of $2X10^{20}$ cm^{-3} were used because some of the experimental data were available for this doping concentration for verification of the emissivity modeling [15]. Temperature range of interest in plasma etching for M-WIP is only 50°-150°C and hence the temperature dependence of optical constants in this temperature range was neglected. Spectral and directional dependence of emissivity was investigated in the spectral range of 2.5 μm to 5.0 μm. This spectral range was selected due to the fact that the product of PtSi detector responsivity and the spectral exitance of a blackbody source, as shown in Figure 27, is effective only in this wavelength range.

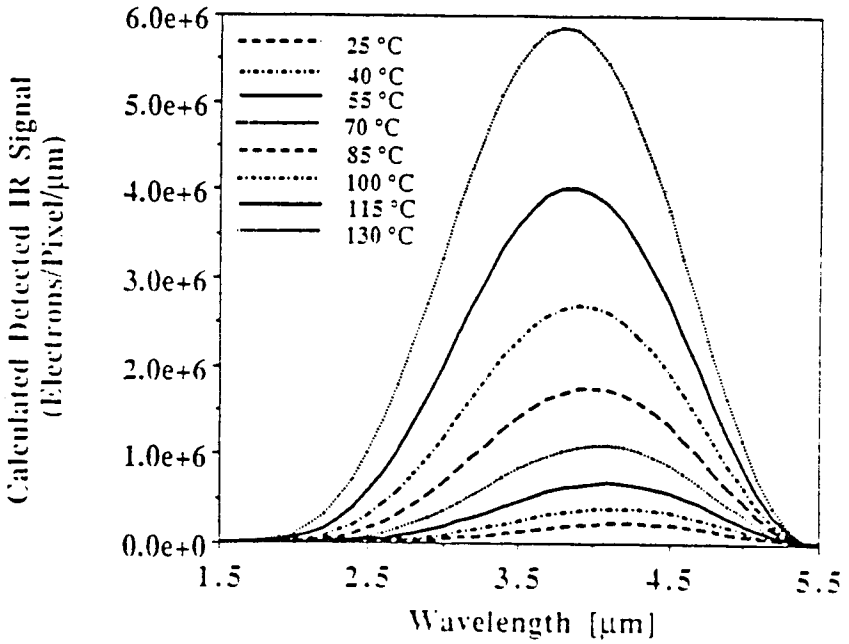

Figure 27 Product of PtSi detector responsivity and the spectral exitance of a blackbody source in the temperature range of 25°C to 130°C.

The first two structures listed in the beginning of this section represent a case of etching of Poly-Si gate material on field oxide in the fabrication of MOS devices. In the first case (see Figure 28(a)), thin Poly-Si and oxide films are present on the back side of the substrate. Figure 28(b) shows the calculated emittance at 3.0 μm, 4.1 μm and 5.0 μm as a function of thickness of the material being etched. This simulation was done at eight different thickness of Poly-Si, starting from 500 nm to 0 nm (i.e. completely removal from the top of SiO_2/Si) in step of around 70 nm. As can be seen from Figure 28(b), end-point of etching can be detected by monitoring change in emissivity at any wavelength in the spectral range of interest. Spectral emissivity in the spectral range of 2500 nm to 5000 nm is plotted for various etched material thicknesses (i.e. Poly-Si and SiO_2) in Figures 28(c) and 28(d). It should be noticed in Figures 28(c) and 28(d) that the emissivity variation is very random in the range of 2500 nm to 3500 nm for different thicknesses. However, between 3500 nm to 5000 nm, emissivity has a quadratic spectral dependence during etching for all thicknesses. This is a very important information for application of Multi-Wavelength Imaging Pyrometry (M-WIP) technique which suggests that a quadratic (2nd order polynomial) dependence of emissivity should be assumed in the emissivity model. Hence, measurements at five wavelengths are sufficient for accurate temperature measurements using M-WIP.

Poly-Silicon	(5000 Å)
SiO_2	(5400 Å)
Si Substrate	(0.5 mm)
SiO_2	(5400 Å)
Poly	(5000 Å)

(a)

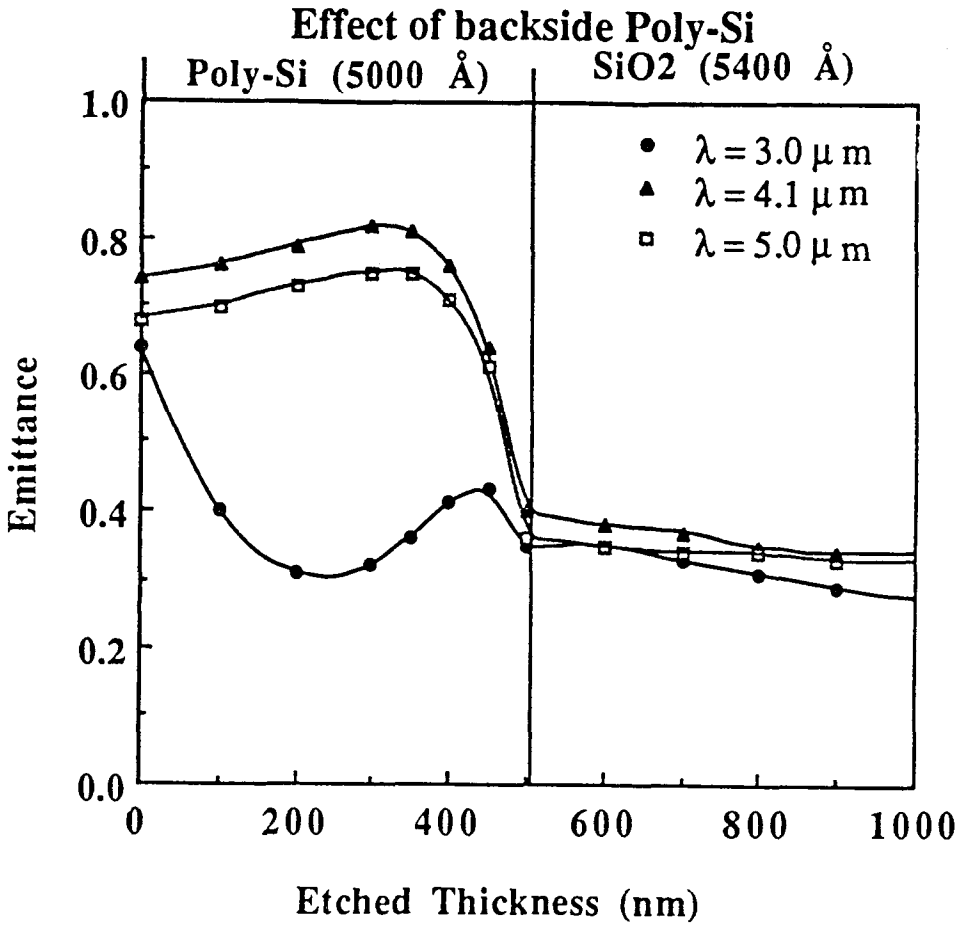

(b)

Figure 28 Calculated emittance at 3.0 μm, 4.1 μm and 5.0 μm as a function of thickness of the material being etched in (b) for the"Poly-Si/SiO_2/Si/SiO_2/Poly-Si " multi-layer structure as shown in (a).

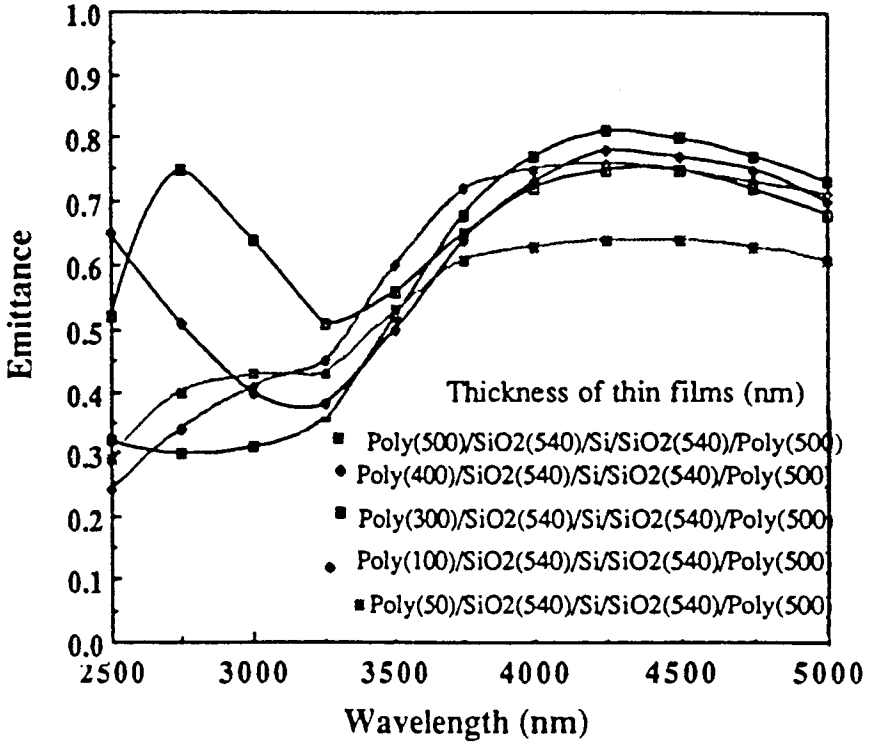

(c)

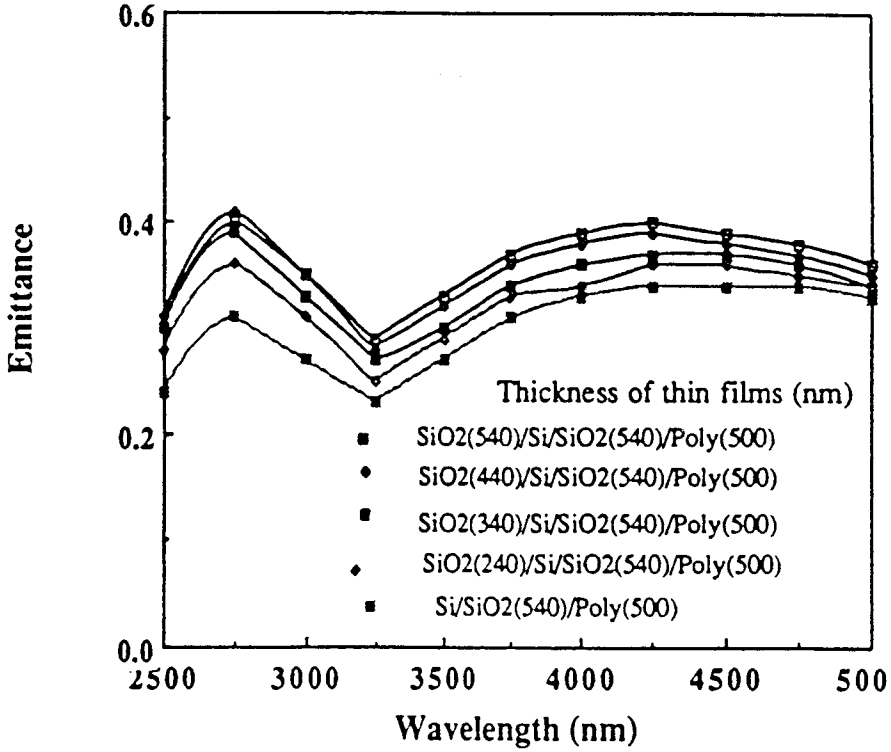

(d)

Figure 28 (cont.) Calculated Spectral emittance within 2.5 μm to 5.0 μm for different thickness of the material being etched in (c) and (d).

In standard IC fabrication procedure, Poly-Si/oxide films are removed from the back side of the substrate prior to plasma etching of Poly-Si film from the front side. The resultant structure is shown in Figure 29(a). Figure 29(b) shows the calculated emittance at 3.0 μm, 4.1 μm and 5.0 μm as a function of thickness of the material being etched for this structure. Comparison of Figures 29(b) and 28(b) shows that emissivity after complete removal of the Poly-Si from the front side is much lower for the case of no Poly-Si/oxide films on the back-side of the substrate. Thus, removing Poly-Si/oxide films from the back-side of the substrate prior to etching drastically improves the end-point detection capability. Calculated spectral emissivity in the spectral range of 2500 nm to 5000 nm is plotted for various etched material thicknesses (i.e. Poly-Si and SiO_2) in Figures 29(c) and 29(d) for the structure shown in Figure 29(a). Spectral dependence of the emissivity for this case is very similar to the case with Poly-Si/oxide films on the back-side and hence the useful spectral range for M-WIP is 3500nm to 5000nm and quadratic dependence of emissivity can be assumed in this spectral range.

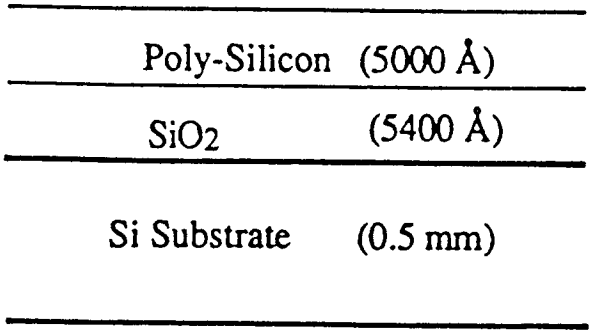

(a)

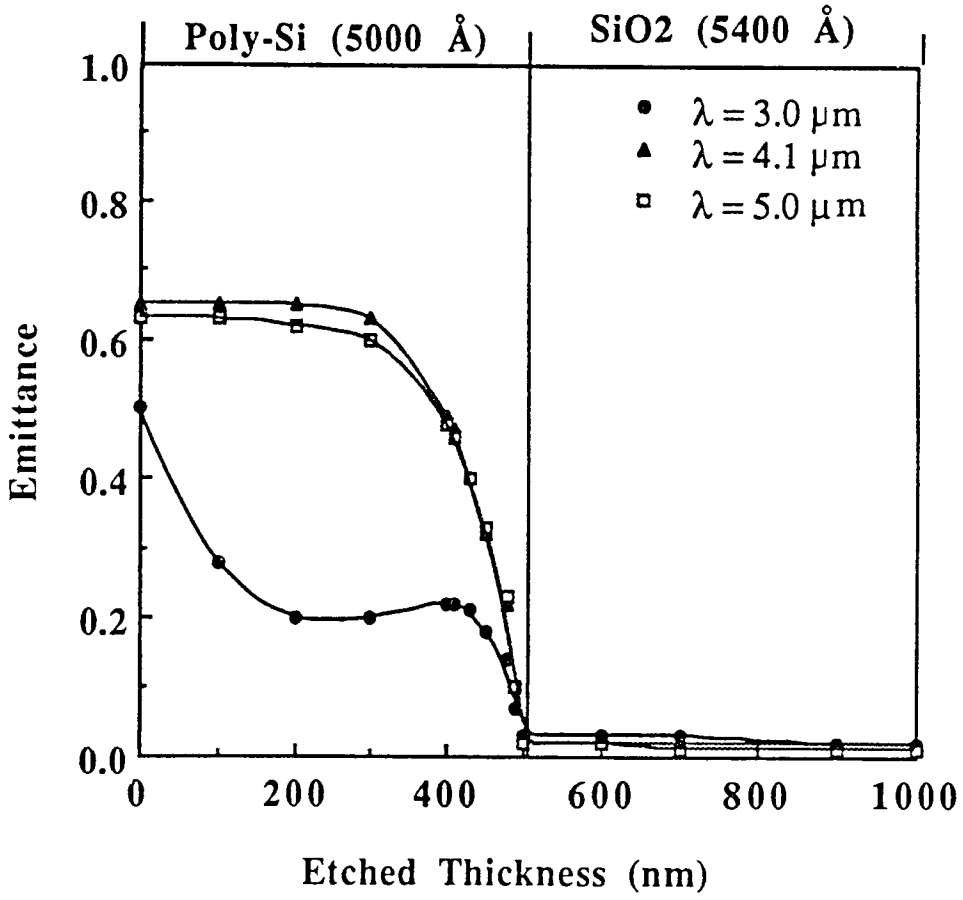

(b)

Figure 29 Calculated emittance at 3.0 μm, 4.1 μm and 5.0 μm as a function of thickness of the material being etched in (b) for the "Poly/SiO_2/Si " multi-layer structure as shown in (a).

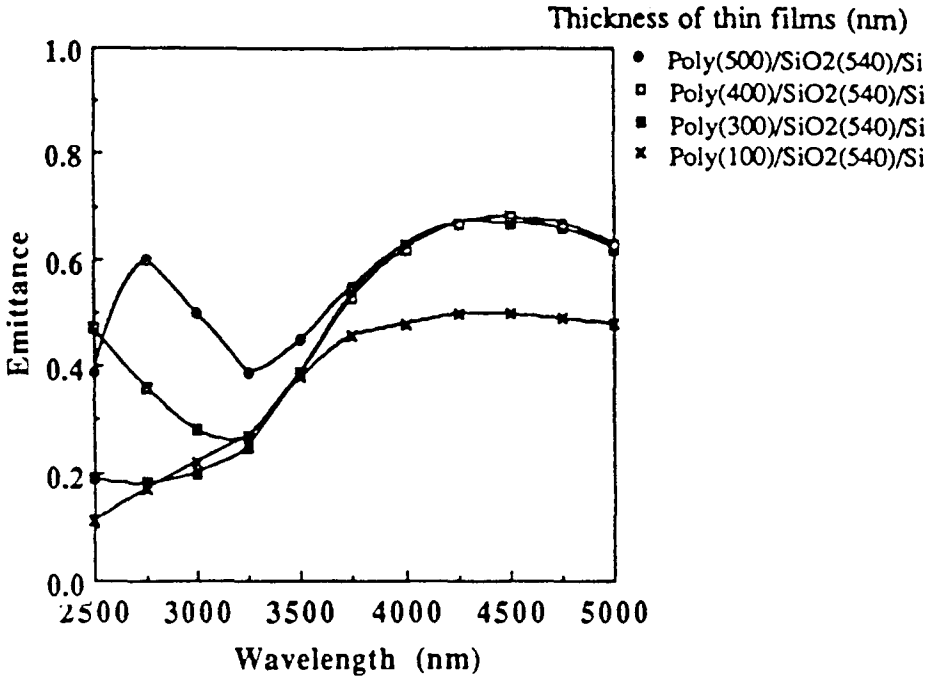

(c)

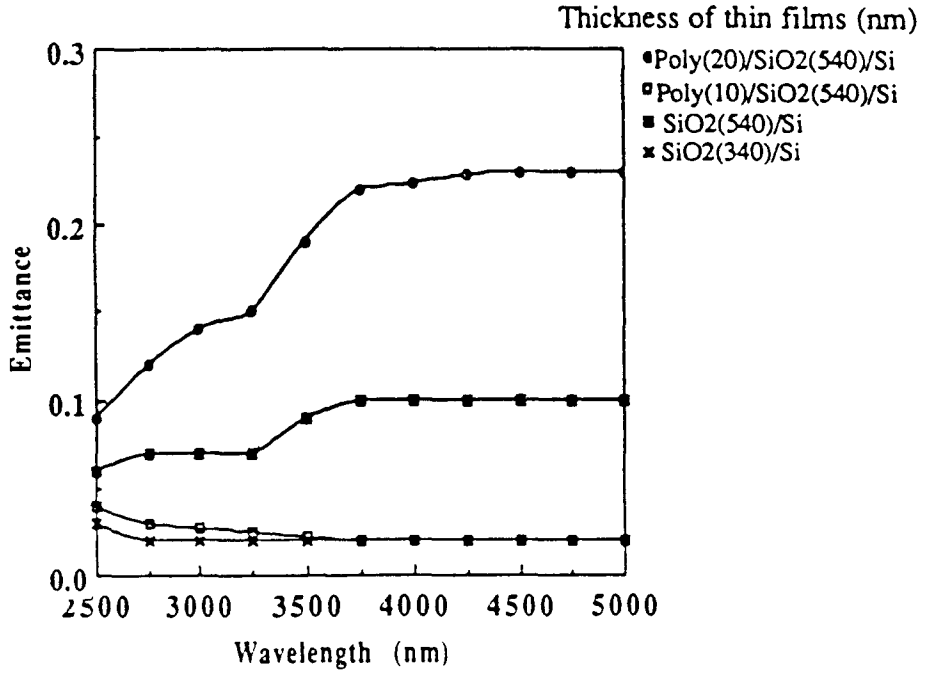

(d)

Figure 29 (cont.) Calculated spectral emittance within 2.5 μm to 5.0 μm for different thickness of the material being etched in (c) and (d).

Some of the emissivity modeling results presented in Figures 28 and 29 were verified using experimental data available from a SEMATECH funded project [15]. This project was based on *in situ* monitoring of wafers by the infrared camera during plasma etching in a single-band (3 to 5 μm with peak-response at 4.1μm) detection scheme. Figure 30 shows the detected infrared signal during the etching of polysilicon film on oxidized wafers with and without films on the backside, etched under identical conditions. These experimental results compare well with the emissivity simulation results in Figures 28(b) and 29(b).

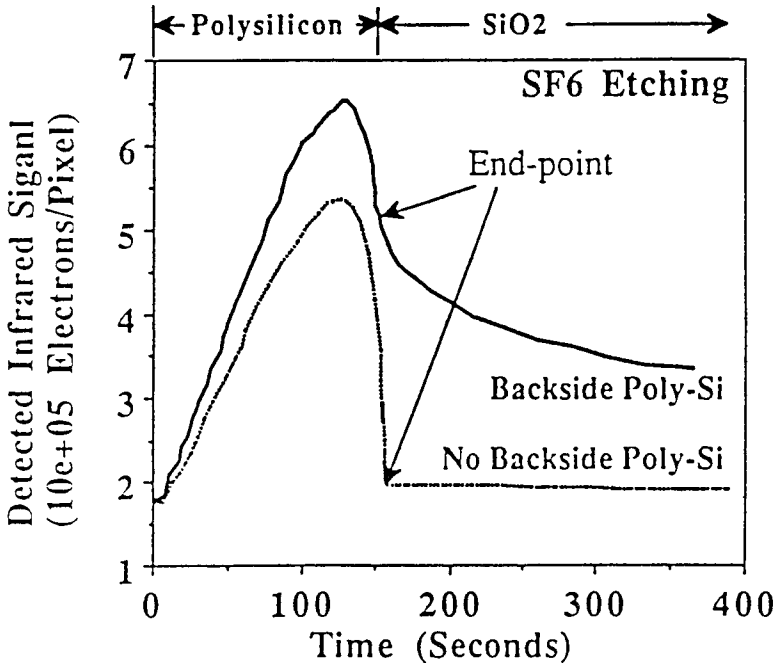

Figure 30 Detected infrared signal during plasma etching of position on oxidized substrate with and without Poly-Si/SiO_2 films on the backside [15].

For the gate definition of MOS structures, Poly-Si is being etched on very thin gate oxides. A multi-layer structure representing this case is shown in Figure 31(a). Also, in present advanced etching tools, normal optical access to the wafer is not possible. In order for M-WIP to be useful in production environment, it is necessary to know the spectral emissivity at certain angle. Figures 31(b) and 31(c) show the calculated emittance at 3.0 μm, 4.1 μm and 5.0 μm as a function of thickness of the material being etched for viewing angles of 0° (normal) and 80° to normal, respectively. It is evident from these figures that end-point of Poly-Si etching can be detected irrespective of underlying oxide thickness and viewing angle. Calculated spectral emissivity for this structure is plotted for various etched material thicknesses (i.e. Poly-Si and SiO_2) in Figures 31(d) and 31(e) for viewing angles of 0° and 80°, respectively. As can be seen from these figures that the spectral behavior of emissivity is very similar for both the angles. For this structure spectral emissivity can be assumed linear within 2500nm to 3200nm and 3700nm to 5000nm spectral range. If radiation measurements are taken within this range using M-WIP, only four different wavelengths are necessary for accurate calculation of temperature.

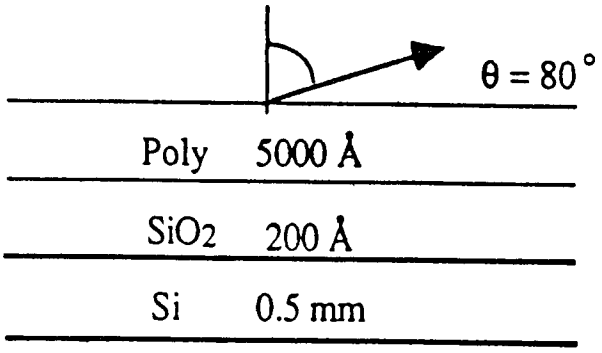

(a)

Figure 31 Poly-Si/SiO2(200 Å)/Si Structure representing Poly-Si etching on gate oxides in (a).

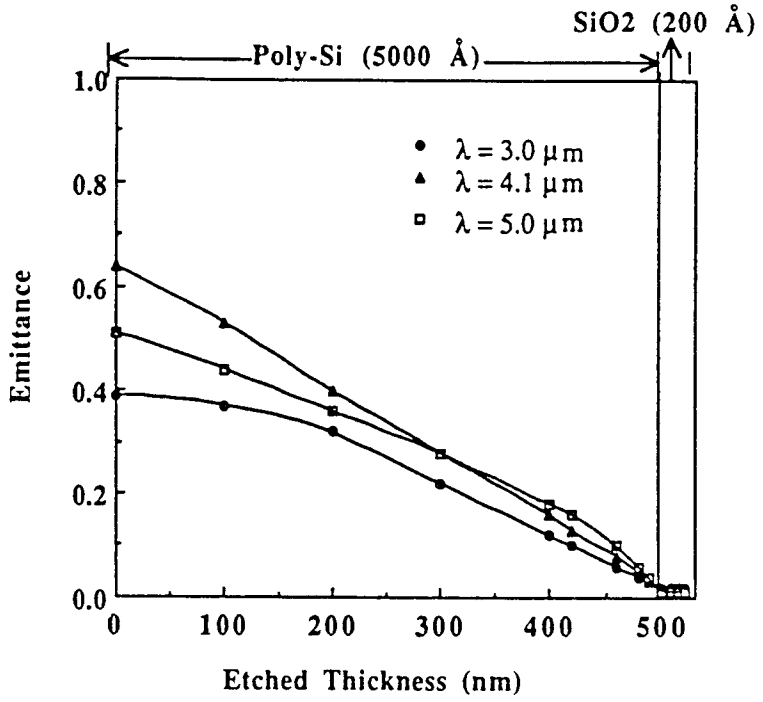

(b)

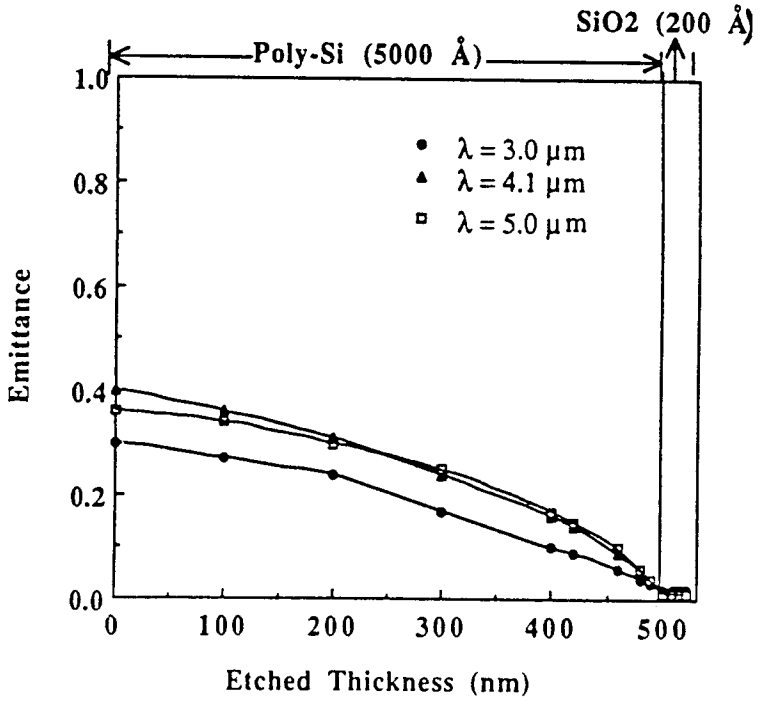

(c)

Figure 31 (Cont.) Calculated emittance at 3.0 μm, 4.1 μm and 5.0 μm as a function of thickness of the material being etched for θ=0° in (b) and for θ=80°in (c) for the "Poly-Si/SiO_2/Si " multi-layer structure as shown in (a).

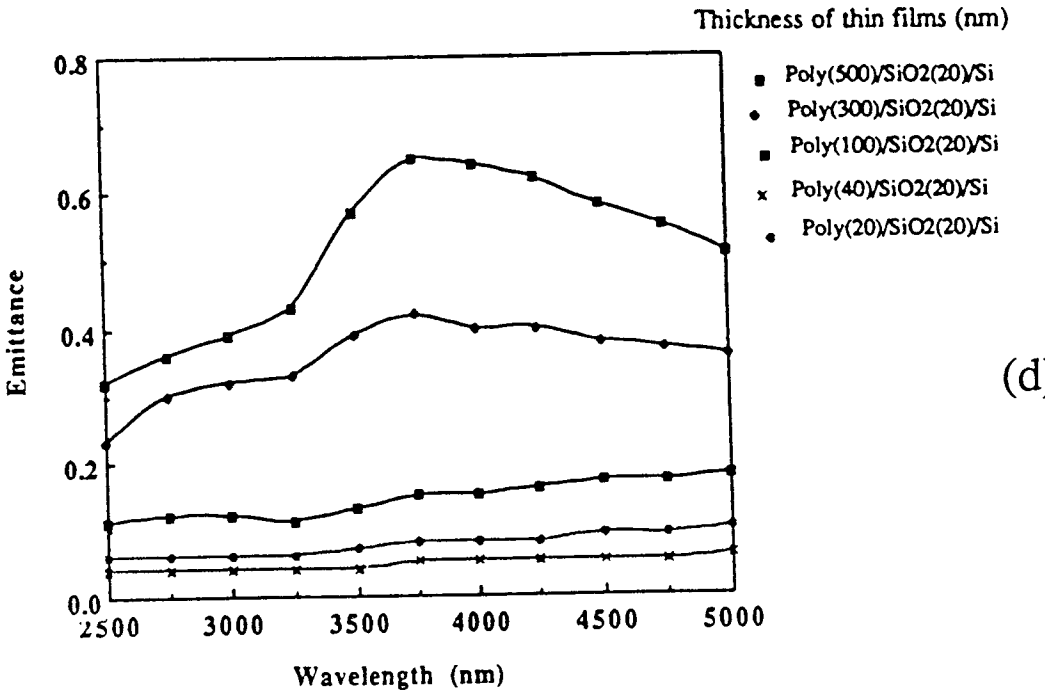

(d)

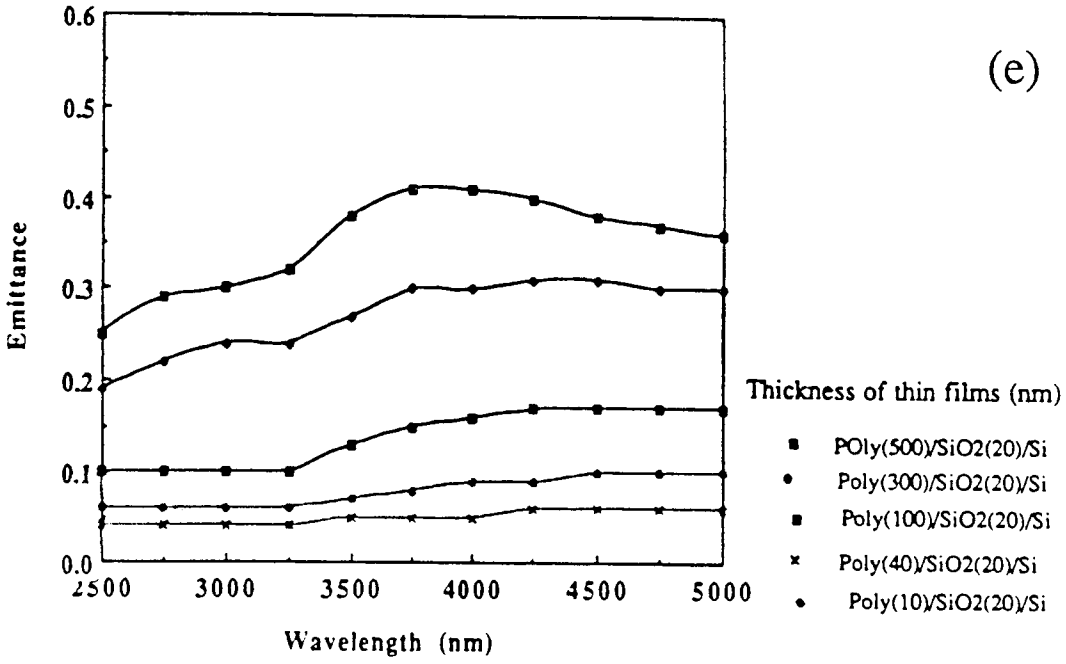

(e)

Figure 31(cont.) Calculated Spectral emissivity within 2.5 μm to 5.0 μm for different thickness of the material emitted at 0°in (d) and at 80° in (e) for the structure shown in (a).

Silicides are extensively used as a gate material in VLSI and ULSI circuit fabrication due to their excellent electrical conductivity. The most common types of Silicides used for this application are $MoSi_2$, WSi_2, $TaSi_2$ and $TiSi_2$. $TaSi_2$ was chosen for our study. Figure 32(a) shows a structure representing etching of $TaSi_2$ on an oxidized Si substrate. The optical data for $TaSi_2$ were obtained from the work published by A. Borghesi et. al. [19]. Figure 32(b) and 32(c) show the calculated emissivity variation at three wavelengths (3.0 μm, 4.1 μm and 5.0μm) during etching of $TaSi_2$ on oxidized (3000 Å) Si for viewing angles of 0° and 80°, respectively. A thick $TaSi_2$ layer represents a metallic surface and the emissivity is constant during initial etching of $TaSi_2$. However, near the interface, a very pronounced emissivity peak is observed. This peak is followed by a sharp drop as the oxide layer is approached. The higher value of emissivity for 80° is due to directional dependence of polarized components as explained in Section 4.3 (see Figure 25). Calculated spectral emissivity for this structure for various etched material thicknesses is plotted in Figures 32(d) and 32(e) for viewing angles of 0° and 80°, respectively. As can be seen from these figures that the spectral behavior of emissivity is very similar for both the angles. For this structure, a quadratic dependence of emissivity can be assumed in the entire spectral range of interest and five wavelengths are required for M-WIP.

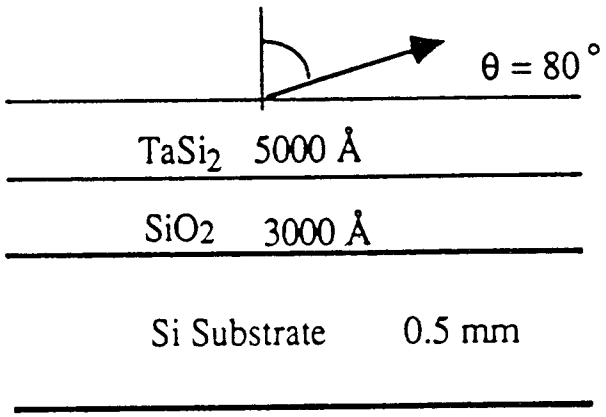

(a)

Figure 32 TaSi2/SiO2/Si structure representing silicide etching on oxidized Si in (a).

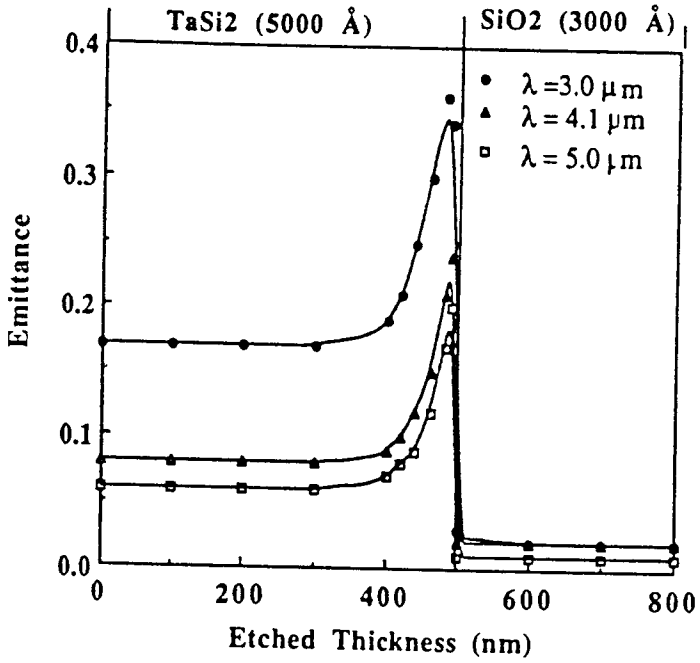

(b)

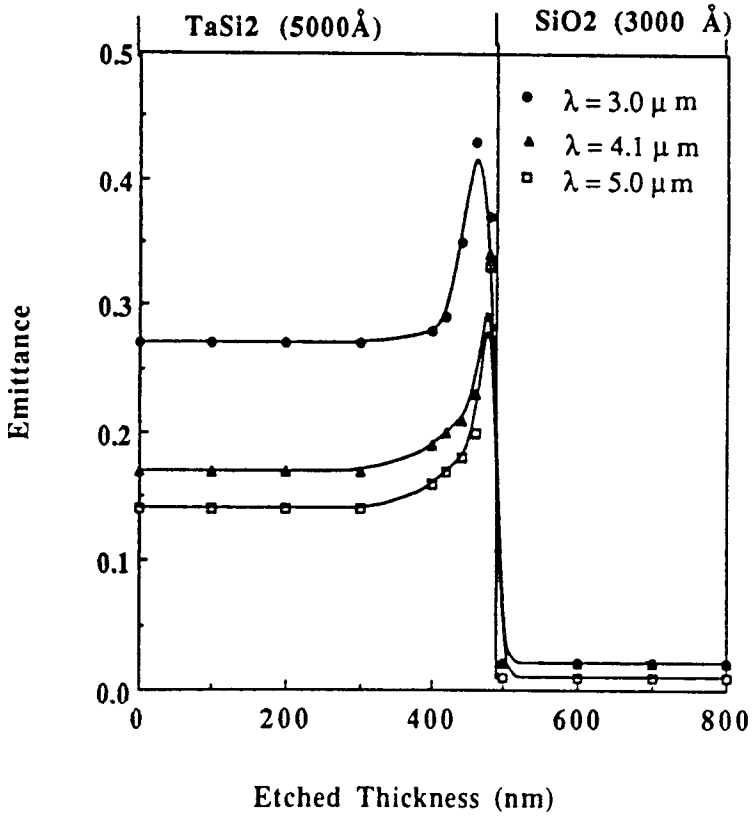

(c)

Figure 32 (Cont.) Calculated emittance at 3.0 μm, 4.1 μm and 5.0 μm as a function of thickness of the material being etched for θ=0° in (b) and for θ=80°in (c) for the "$TaSi_2/SiO_2/Si$ " multi-layer structure as shown in (a).

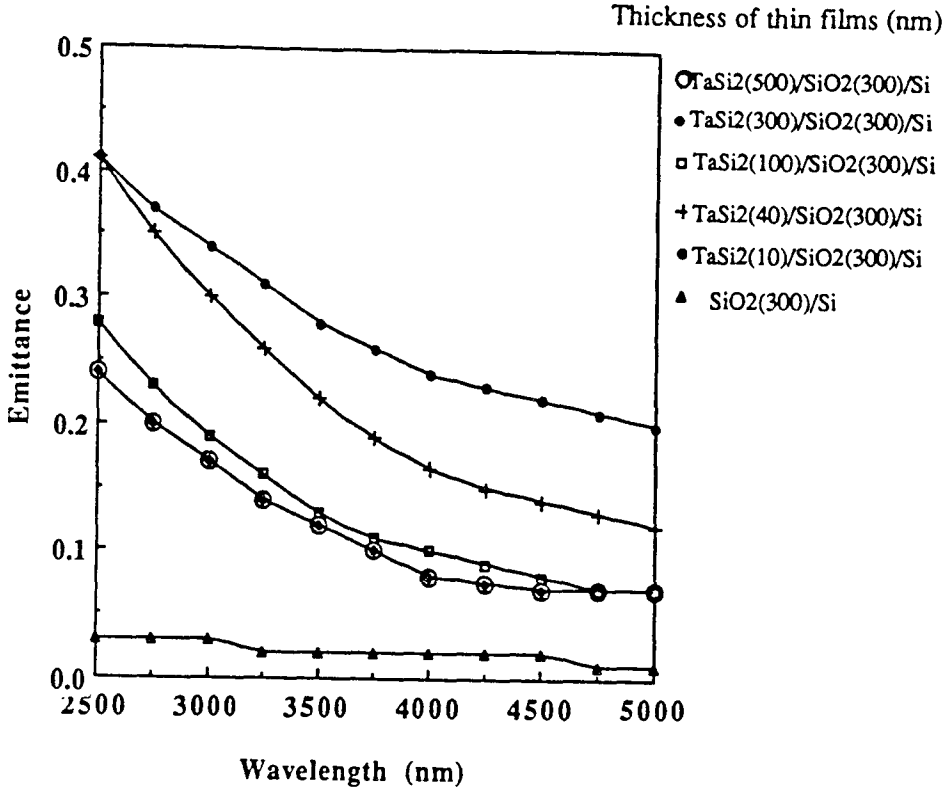

(d)

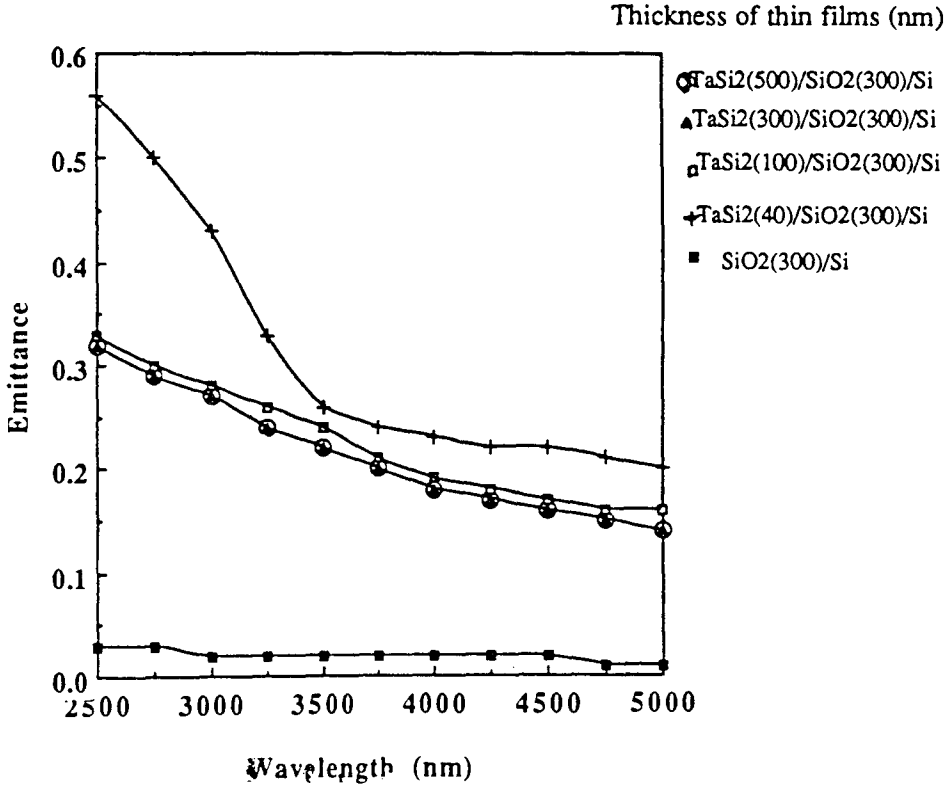

(e)

Figure 32(cont.) Calculated spectral emissivity within 2.5 μm to 5.0 μm for different thickness of the material, emitted at 0° in (d) and emitted at 80° in(e) for the structure shown in Fig. 32a.

A recent trend in fabrication of VLSI circuits is to use a refractory metal silicide on top of Poly-Si. This approach (called polyside) combines the advantages of the polysilicon and silicide technology and reduces the sheet resistance while preserving the polysilicon-SiO_2 interface. A structure representing this approach is shown in Figure 33(a). Figure 33(b) shows the calculated emissivity variation at three wavelength (3.0 μm, 4.1 μm and 5.0μm) as a function of film thickness for this polyside structure for normal viewing. It can be seen from this figure that the drastic change in emissivity at the $TaSi_2$/Poly-Si and Poly-Si/SiO_2 interfaces allows end-point detection. Calculated spectral emissivity for this structure is plotted for various etched material thicknesses in Figures 33(c) and 33(d). It can be inferred from these figures that the emissivity for this structure is linear within spectral range of 3700 nm to 5000nm, however it quadratic dependence between 2500 nm and 3700 nm.

In summary, emissivity modeling presented in this section allows determination of spectral range and emissivity model for M-WIP for various plasma etching processes.

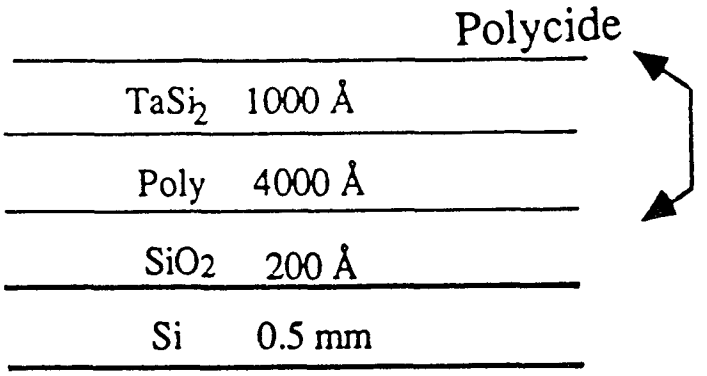

(a)

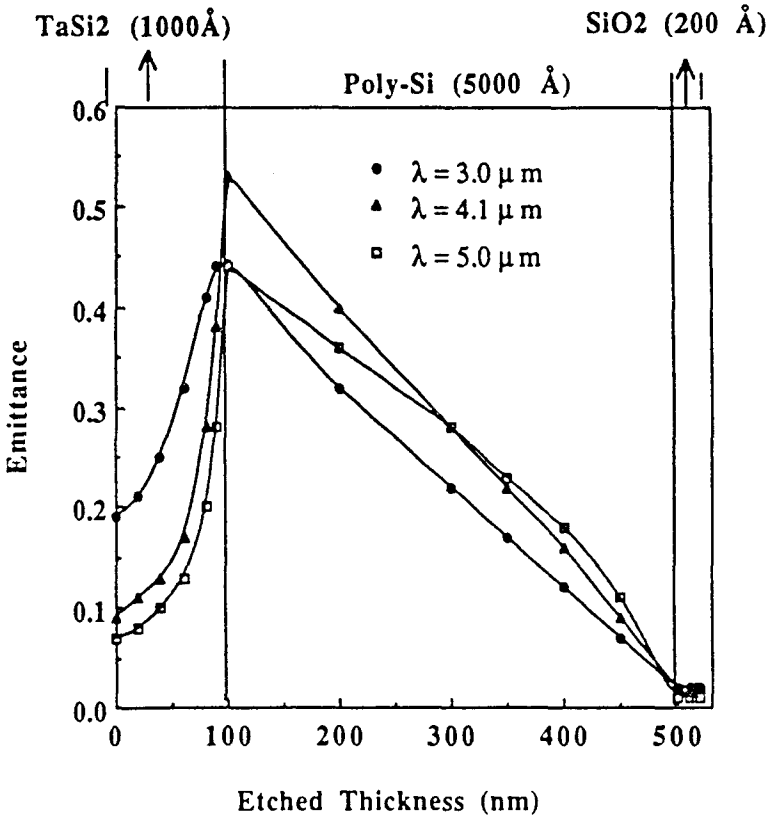

(b)

Figure 33 Calculated emittance at 3.0 μm, 4.1 μm and 5.0 μm as a function of thickness of the material being etched in (b) for the "$TaSi_2$/Poly-Si/SiO_2/Si " multi-layer structures shown in (a).

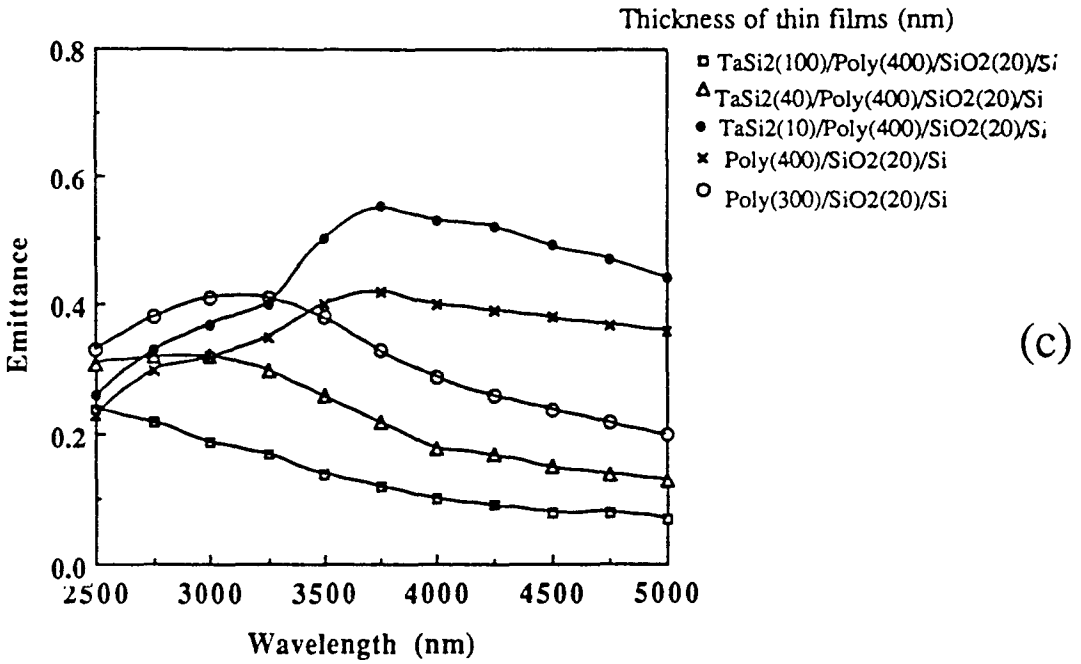

(c)

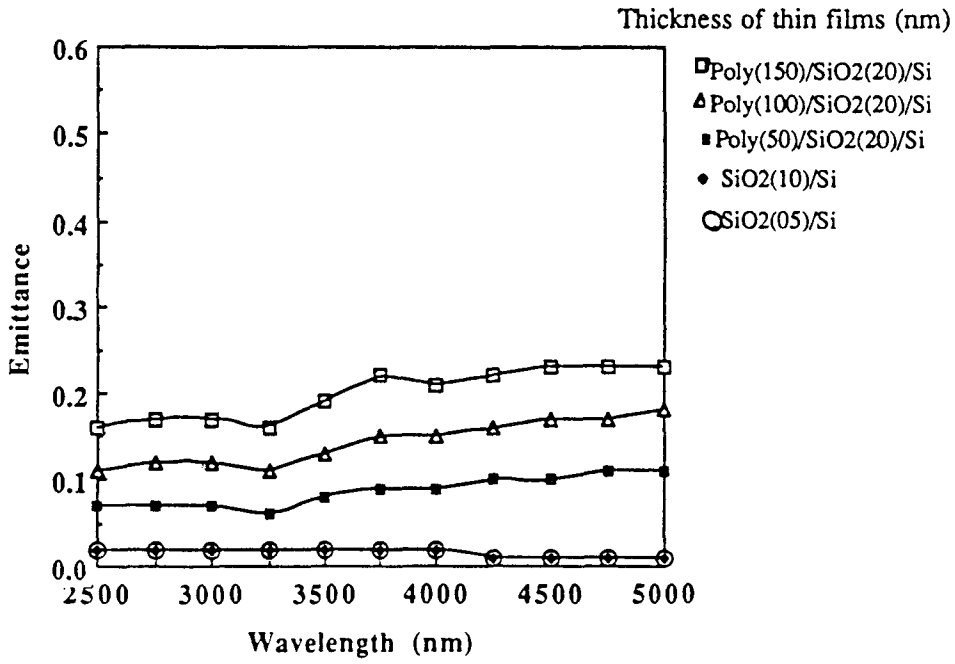

(d)

Figure 33 (cont.) Calculated spectral emittance within 2.5 μm to 5.0 μm for different thickness of the material in (c) and (d) for the multi-layer "$TaSi_2$/Poly-Si/SiO_2/Si " structure as shown in (a).

CHAPTER 5

CONCLUSIONS AND SUGGESTIONS FOR FUTURE WORK

5.1 Conclusions

This thesis research covered two different topics related to development of Multi-Wavelength Imaging Pyrometry (M-WIP). The objectives of this thesis research were : (a) design of a mask for narrow-band striped filters and (b) the development of the emissivity modeling for multi-layer thin film structures, were successfully carried out.

A four layer mask was designed and fabricated for defining multi-wavelength striped-filters compatible with focal plane array to facilitate multiple-wavelength measurement for the M-WIP system. The first mask can be used for chrome patterning, while the other three masks can be used to deposit three different wavelength filters. A special mask design would allows twelve distinct striped-filter geometries including two wavelength and three wavelength horizontal (80 μm spacing) and vertical stripes (40 μm spacing), single wavelength filters and various test structures to be fabricated on a 4-inch silicon substrate. The fabricated mask will be used for a detailed feasibility study on fabrication of multiple wavelength striped filters.

A detailed study of spectral (2.5 μm to 5.0 μm) and directional (0° and 80° from the normal of surface) emissivity variation of thin-film multilayer structure, using the developed model, was done for several important structures commonly used in plasma etching. These multi-layer structures are polycrystalline silicon (Poly-Si) on thin and thick oxides, silicides on thick oxides and polysides on thin oxides. For the Poly-Si on thick oxide, it was found that the emissivity is quadratic with wavelength between 3.5 μm to 5.0 μm during etching for all thicknesses; however it has large variation in the spectral range of 2.5 μm to 3.5 μm for different etched thicknesses and is more difficult to model.

For the Poly-Si on thin oxide structure, it was found that emissivity is linear with wavelength from 2.5 μm to 3.2 μm and from 3.7 μm to 5.0 μm. For silicide on thick oxide, the emissivity was quadratic with wavelength in the entire spectral range of interest (i.e. 2.5 μm to 5.0 μm), while for polyside on thin oxide, the emissivity was linear with wavelength in the spectral range of 3.7 μm to 5.0 μm; however it was quadratic from 2.5 μm to 3.7 μm.

5.2 Suggestions for Future Work

After the initial feasibility study of fabricating three-wavelength striped filter is done, the mask design presented in this thesis can be easily modified so that multi-striped (more then three wavelength) filters can be fabricated. The dependence of n on λ, filter/detector separation and diffraction effect should be taken into account in future design for imaging radiometry applications.

Emissivity modeling work presented in Chapter 4 can be extended to other processing applications such as sputtering, evaporation and PECVD. However, for high temperature applications such as RTP and CVD, the temperature dependence of optical constants should be included in the model.

APPENDIX A

Figures for Striped Filters Mask

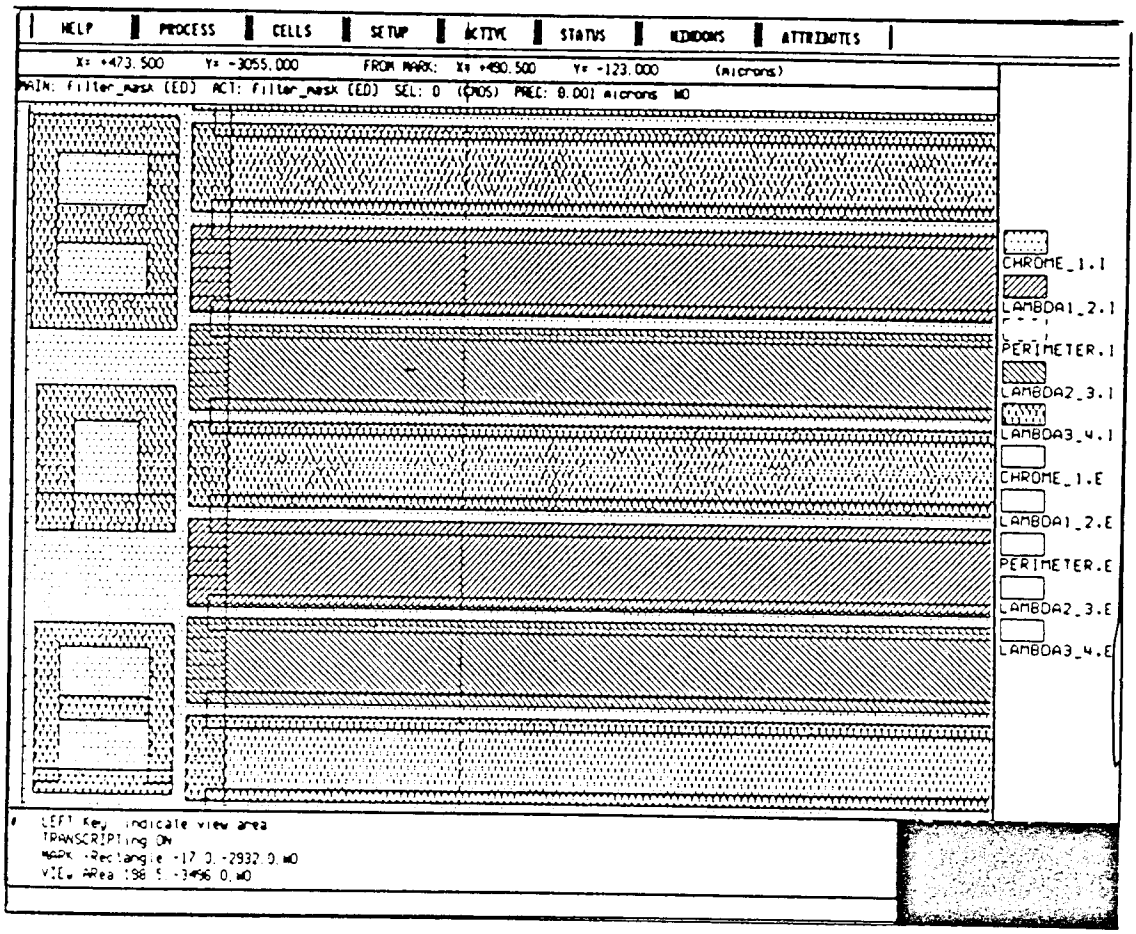

Filter 80B

Filter strip width = 70 μm Separation between stripes= 10μm

Chrome width = 30 μm Separation between stripes =50μm

Overlap between chrome strip and filter stripes = 10μm

Figure 1 Layout of three-wavelength horizontal striped filter (80B)
Right end side indicates process layers (only four with patterned) used in this layout.

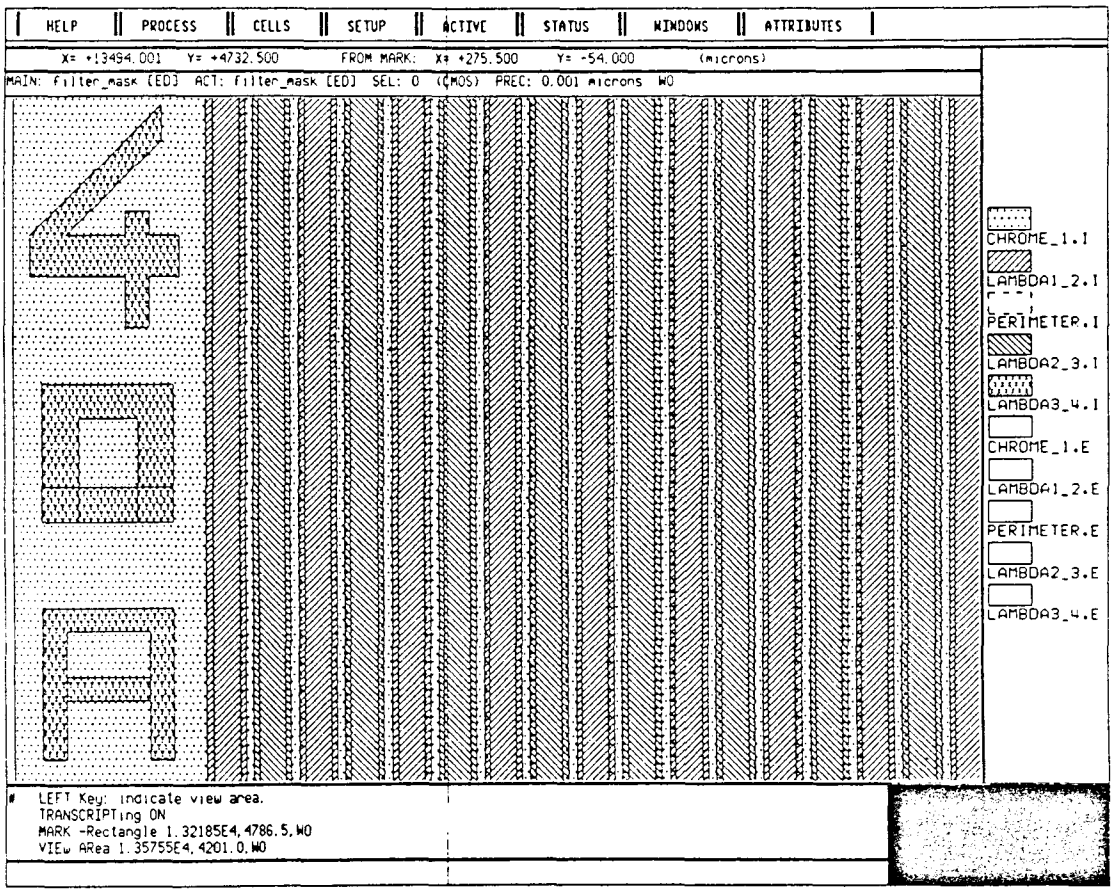

Filter 40A ;

Filter strip width = 33 μm Separation between stripes 07μm

Chrome width = 17 μm Separation between stripes= 23μm

Overlap between chrome strip and filter stripes = 05μm

Figure 2 Layout of two-wavelength vertical striped filter (40A).

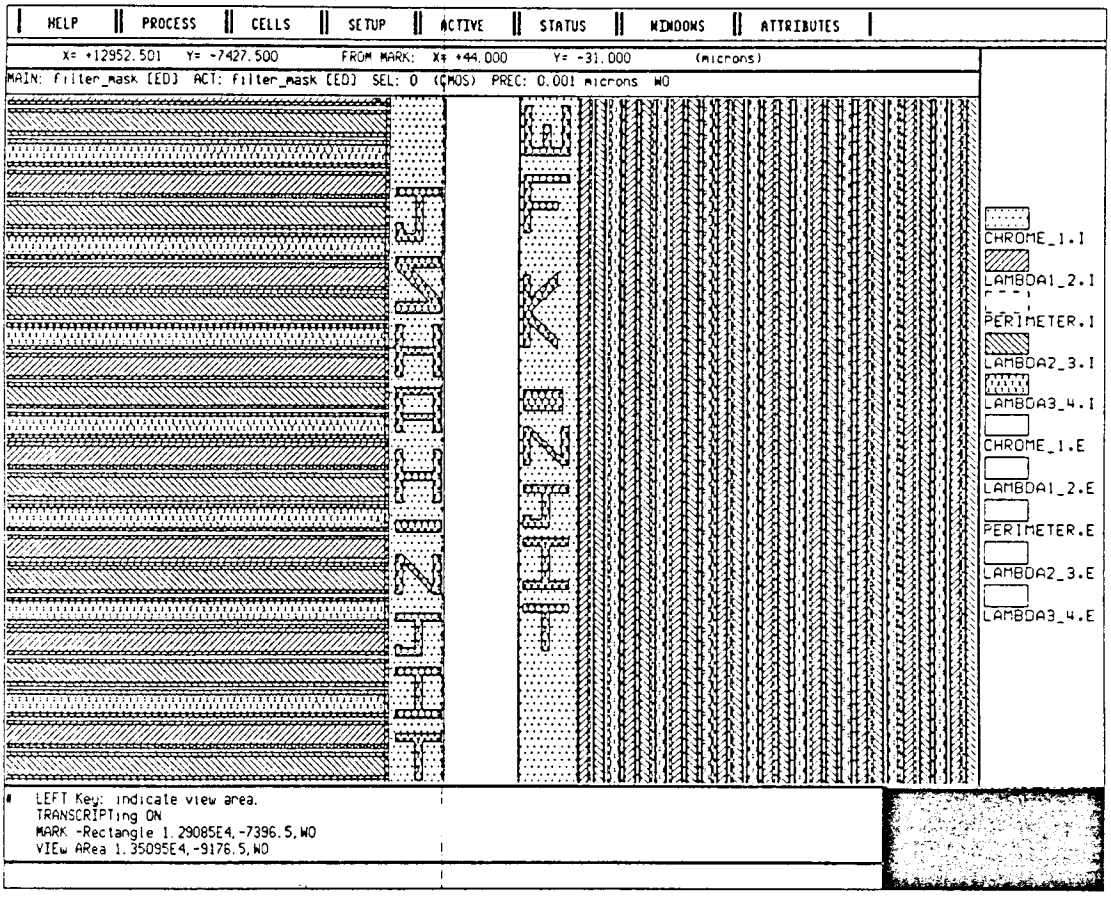

Figure 3 View graph shows name of author and his advisor name written at each side of filters using chrome1, i.e. 1st layer.

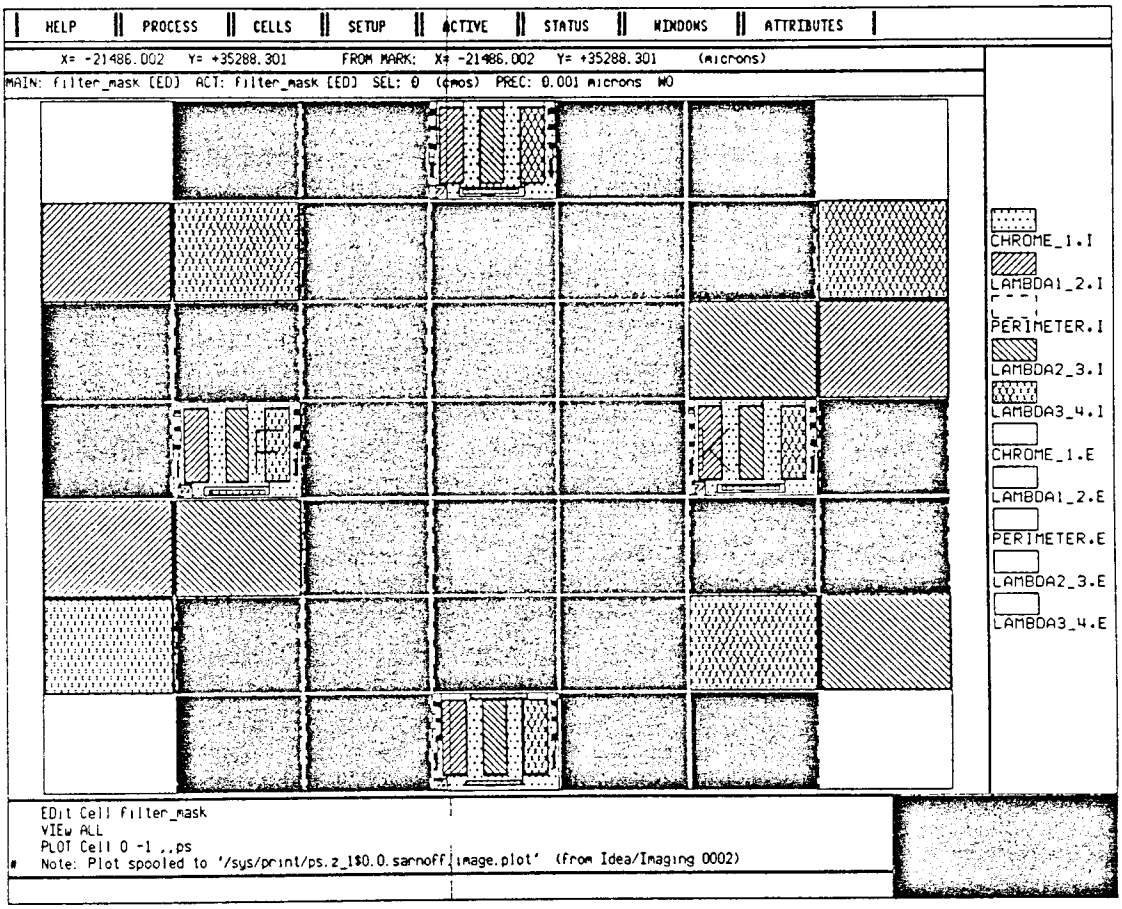

Figure 4 Center portion of final mask views after TRANSLATION from GDSII file (filter.gds).

APPENDIX B

Optical Constants (n and k) of Semiconductor Materials Within 2.0μm to 5.0μm Range

Material	λ	n	k	Source
Si	2.0	3.449	1.07e-4	Ref. 22
	2.437	3.443	1.07e-4	
	2.500	3.442	1.07e-4	
	2.714	3.439	1.07e-4	
	3.00	3.436	2.5e-9	
	3.303	3.433	2.5e-9	
	3.419	3.433	2.5e-9	
	3.500	3.432	2.5e-9	
	3.800	3.430	1.3e-8	
	4.00	3.429	1.3e-8	
	5.00	3.426	1.9e-7	
SiO2	2.053	1.520	1.66e-5	Ref. 22
	2.058	1.520	1.66e-5	
	2.300	1.516	1.66e-5	
	2.500	1.512	1.66e-5	
	2.600	1.510	1.66e-5	
	3.00	1.500	1.66e-5	
	3.500	1.485	1.66e-5	
	4.00	1.466	1.66e-5	
	4.200	1.457	1.66e-5	
	4.40	1.448	1.66e-5	
	4.60	1.437	1.66e-5	
	4.8	1.425	1.66e-5	
	5.0	1.412	1.66e-5	

Optical Constants (n and k) of Semiconductor Materials (cont..)

Material	λ	n	k	Source
Poly-Si	2.0	3.050	0.040	Ref. 18
	2.250	2.950	0.121	
	2.500	2.830	0.159	
	2.750	2.650	0.216	
	3.00	2.530	0.250	
	3.25	2.410	0.284	
	3.50	2.260	0.445	
	3.75	2.100	0.656	
	4.00	1.930	0.795	
	4.25	1.820	1.000	
	4.50	1.700	1.250	
	4.75	1.680	1.430	
	5.00	1.650	1.790	
TaSi2	2.060	2.00	4.0	Ref. 21
	2.250	2.20	4.8	
	2.480	2.30	5.2	
	2.880	2.40	6.5	
	3.350	2.60	8.0	
	4.00	2.80	11.0	
	4.960	3.40	14.5	
Al	2.0	2.15	20.7	Ref. 22
	2.254	2.62	23.3	
	3.0	4.24	30.6	
	3.1	4.45	31.5	
	3.30	4.88	33.4	
	3.54	5.44	35.6	
	4.0	6.43	39.8	
	4.5	7.61	44.3	
	5.0	8.67	48.6	

REFERENCES

1. M.A. Khan, C. Allemand and T.W. Eagar, "Non contact Temperature Measurement I: Interpolation Based Techniques," *Rev.Sci.Instrum.*, Vol. 62, No. 2, February, 1991.

2. D.P. Dewitt and F.P. Incropera, "Physics of Thermal Radiation," in Theory and Practice of Radiation Thermometry, John Wiley & Sons, New York, 1988.

3. M.A. Khan, C. Allemand and T.W. Eagar, "Non contact Temperature Measurement II: Least Squares Based Techniques," *Rev.Sci.Instrum.*, Vol. 62, No. 2, February, 1991.

4. Bevington, Data Reduction and Error Analysis for the Physical Sciences, McGraw-Hill Book Co., New York, 1969.

5. M. Kaplinsky, "Application of Imaging Pyrometry for Remote Temperature Measurements," Masters Thesis, New Jersey Institute of Technology, January 1993.

6. W.F. Kosonocky, "Review of Infrared Image Sensors with Schottky-Barrier Detectors", *Optoelectronics*, 6,2,173-203, 1991.

7. Raster Graphics Handbook, Conrac Corporation, CA, 1987.

8. N. McCaffrey, "Design of a 320x122 MWIR-CCD PtSi-Si Imaging Radiometer with Automatic Optical Integration Time Control," Master's Thesis, New Jersey Institute of Technology, May, 1993.

9. S. Amin, "Design, Fabrication and Characterization of Infrared Filter," Masters Thesis, New Jersey Institute of Technology, October, 1993.

10. D.P. Dewitt and J.C. Richmond, "Thermal Radiative Properties of Materials," in Theory and Practice of Radiation Thermometry, John Wiley & Sons, New York, 1988.

11. Private conversation with Dr. W.F. Kosonocky.

12. Mentor Graphics "Chip Graph User's Manual," Version 6.1, Vol.1&2, 1988.

13. H.O. McMahon, "Thermal Radiation from Partially Transparent Reflecting Bodies," *Journal of The Optical Society of America,* Vol.40, No. 6, June, 1950.

14. P.W. Kruse, L.D. McGlauchlin and R.B. McQuistan, Elements of Infrared Technology, p.14, New York, 1962.

15. V. Patel, "Characterization of Advanced Plasma Etching Reactors Using Novel Diagnostic Tools," Doctoral Thesis, New Jersey Institute of Technology, May 1993.

16. R. Gardon, "The Emissivity of Transparent Materials," *J. Am.Ceram. Soc.*, Vol. 39, No. 8, pp.278-287, 1956.

17. R. Gardon, "A Review of Radiant Heat Transfer in Glass," *J. Am. Ceram. Soc.*, Vol. 44, No. 7, p.305-312, 1961.

18. H. Macleod, "Thin-Film Optical Filters", McGraw Hill Publishing Co., NY, 1989.

19. A. Borghesi, L. Nosenzo and A. Piaggi, "Optical Properties of Tantalum Disilicide Thin Films," *Physical Review B*, Vol. 38, No.15, November, 1988.

20. E.D. Palik, "Handbook of Optical Constants of Solids," Academic Press, 1985.